IN-01

198147

P- 45

Some VTOL Head-Up Display Drive-Law Problems and Solutions

Vernon K. Merrick

November 1993

NASA

National Aeronautics and
Space Administration

Some VTOL Head-Up Display Drive-Law Problems and Solutions

Vernon K. Merrick, Ames Research Center, Moffett Field, California

November 1993

NASA

CONTENTS

iii

PAGE __ii__ INTENTIONALLY BLANK

SYMBOLS

To create a degree of order, the following rules have been adopted in the assignment of mathematical symbols to the various quantities.

- All variables are designated by lower case symbols (Roman or Greek).

- With the exception of the acceleration due to gravity, g, all constants are designated by upper case symbols (Roman or Greek).

- A hat over a quantity (e.g., $\hat{x}$) denotes that the quantity has been normalized. Quantities associated with the acquiring curve are normalized by the acquiring curve length, L, and quantities associated with the blending curve are normalized by the true circle radius, $\bar{R}_l$.

- With the exception of V'_w (adopted to conform with ref. 2), a primed quantity (e.g., x') denotes one that has been differentiated with respect to the range, d.

- A dot over a quantity (e.g., $\dot{x}$) denotes differentiation with respect to time.

- Vector quantities are shown boldface (e.g., $\mathbf{r}$).

The symbols are divided into the following four categories:

1 Input variables (either from sensors or precomputed and stored).

2. Constant inputs (set by the pilot or frozen at flightpath select).

3. Derived variables used in the description of the flightpath and guidance laws.

4. Derived constants used in the description of the flightpath and guidance laws.

Input Variables

h	aircraft altitude, feet (ft)
$\dot{h}$	vertical velocity of aircraft's center of gravity (c.g.), feet per second (ft/sec)
v_t	aircraft groundspeed, ft/sec
$\dot{v}_t$	aircraft acceleration along ground track, ft/sec^2
v_x, v_y	horizontal longitudinal and lateral speeds, ft/sec
$\dot{v}_x, \dot{v}_y$	horizontal longitudinal and lateral accelerations, ft/sec^2
$\hat{x}$	normalized blending-curve ordinate
x_a, y_a	aircraft coordinates in the landing-pad coordinate system, ft
δ_t	throttle position, degrees (deg)
δ_{tc}	throttle compensation parameter, deg
δ_x, δ_y	longitudinal and lateral pilot control inputs, deg
ζ	direction of ghost aircraft relative to real aircraft, deg
θ	aircraft pitch angle, deg

σ_w	aircraft vertical damping parameter, 1/sec
σ_x, σ_y	aircraft horizontal translational damping parameters, 1/sec
ϕ	aircraft roll angle, deg

Input Constants

$C_{\dot\theta}, C_{\dot\phi}$	pitch and roll rate sensitivity to pilot control inputs
D_c	nominal length of final flightpath segment, ft
D_f	threshold range, ft
D_x, D_y	aircraft pitch and roll damping constants, 1/sec
E_q	heading of head-up-display (HUD) flightpath symbol at flightpath select, deg
g	acceleration due to gravity, ft/sec^2
H	hover altitude, ft
H_{ri}	aircraft altitude at guidance select, ft
K_{ab}	ratio of lengths of acquiring curve and initial straight segment
K_ϵ	flightpath-symbol lateral-drive scale factor
$K_{\delta_x}, K_{\delta_y}$	control-input gains, feet per inch second (ft/in. sec)
$\hat{L}_1$	normalized distance along acquiring curve, measured along x-axis, where the angle of bank changes sign (fig. 6)
M_f, H_f	azimuth and elevation of a fixed point in space far ahead of the aircraft, deg
$R_{l(min)}$	nominal minimum radius of horizontal flightpath circles, ft
R	radius, ft
R_v	radius of vertical flightpath circle, ft
S_x, S_y	touchdown or station-keeping point coordinates in the landing-pad reference frame, ft
T_2	control-input washout time constant, sec
$T_{\dot v}$	horizontal-tracking time constant, sec
V_{xf}	desired value of v_x at threshold range, D_f, ft/sec
$\bar{X}_u$	effective value of sign reversed slope of speed-versus-range line of reconfigured aircraft, 1/sec
Γ	approach flightpath angle, deg
ΔD_{ac}	minimum desirable distance along curved segment of flightpath, ft
ΔT_g	general ghost lead time, sec
$\bar{N}_{0(min)}$	minimum permitted value of $\bar\nu_0$, deg
$\hat{\Upsilon}_p$	normalized maximum length of portion of ordinate of blending curve replacing a portion of a straight segment
$\hat{\Upsilon}$	normalized length of portion of ordinate of blending curve replacing a portion of a straight segment
Ψ	landing-pad heading, deg
Ψ_f	heading of final flightpath segment, deg
Ω_0	translational velocity response frequency, radians/sec (rad/sec)

Derived Variables

b_x, b_y	coordinates of point B in landing-pad system prior to flightpath select, ft
d	range to touchdown or station-keeping point measured along synthesized flightpath, ft
d_r	range at which aircraft should be reconfigured, ft
l_c	distance from aircraft to center of flightpath circle, ft
$\hat{\dot{h}}_c$	quickened vertical velocity, ft/sec
h_g	altitude of ghost aircraft, ft
h_r	altitude of reference flightpath at aircraft's range, ft
i	indicates right ($i = +1$) or left ($i = -1$) flightpath circle prior to flightpath select
k_{wg}	ghost lead blending gain
k_{δ_t}	throttle washout gain, ft/sec deg
l_{ac}	distance of aircraft from tangent point C (fig. A-3) of circle with final straight segment, ft
$\mathbf{r}_a$	vector position of real aircraft, ft
$\mathbf{r}_g$	vector position of ghost aircraft, ft
r_l	instantaneous circle radius, ft
r_{ll}	radius of appropriate circle prior to flightpath select, ft
r_{llx}, r_{lly}	coordinates of appropriate circle in landing-pad reference frame prior to flightpath select, ft
s	Laplace transform variable, 1/sec
$\hat{s}(\hat{x})$	nondimensional distance along blending curve from origin (fig. 5)
$\hat{s}(\hat{x}_p)$	nondimensional distance along blending curve from origin to foot of perpendicular from aircraft to blending curve (fig. 5)
$\hat{v}_x, \hat{v}_y$	smoothed estimates of horizontal translational accelerations, ft/sec^2
$\hat{v}_{xc}, \hat{v}_{yc}$	commanded horizontal translational velocities, ft/sec
$\dot{v}_{xr}$	reference longitudinal acceleration, ft/sec^2
x, y	coordinates of acquiring curve, ft
x_f, y_f	HUD coordinates of a fixed point in space with azimuth and elevation of M_f and H_f, respectively, deg
$\hat{x}, \hat{y}$	nondimensional coordinates of blending curve (fig. 5) or acquiring curve (fig. 6)
$\hat{x}_a, \hat{y}_a$	nondimensional coordinates of aircraft in $\hat{x}, \hat{y}$ axes system (fig. 5)
$\hat{x}_p, \hat{y}_p$	nondimensional coordinates of foot of perpendicular from aircraft to blending curve in $\hat{x}, \hat{y}$ axes system (fig. 5)
x_{1a}, y_{1a}	coordinates of aircraft in an axis system with origin at center of flightpath circle and x-axis parallel to final flightpath segment, ft
x_{2a}, y_{2a}	coordinates of aircraft in an axis system with origin at point B (fig. B-1) and x-axis parallel to initial flightpath segment, or with origin at point S and x-axis along final flightpath segment, ft
γ_t	reference flightpath angle at aircraft's position, deg
δh	altitude error relative to reference glide slope, ft
δx_g	general ghost lead distance, ft
δx_{gh}	ghost lead distance for vertical tracking, ft
δy	lateral distance of aircraft from reference flightpath track, ft
$\delta \hat{y}$	nondimensional perpendicular distance from aircraft to blending curve (fig. 5)

$\delta\psi_i$	heading of initial flightpath segment relative to x-axis of landing pad prior to flightpath select, deg
ϵ_q	heading of flightpath relative to heading of aircraft prior to flightpath select, deg
$\hat{\imath}$	nondimensional incremental distance between $\hat{x}_p$ and $\hat{x}_a$
μ_g, η_g	azimuth and elevation of ghost aircraft, deg
ν	angle subtended at center of reference flightpath circle by remaining arc of circular flightpath segment, deg
ν_0	nominal angle subtended at center of reference flightpath circle by entire circular flightpath segment, deg
$\bar{\nu}_0$	angle between line AC (fig. A-2) and final straight segment, deg
$\bar{\nu}_{0l}$	limited value of $\bar{\nu}_0$, deg
ρ	radius of curvature of reference flightpath track, ft
$\hat{v}$	nondimensional parameter defining length of blending curve prior to flightpath select
ϕ_g	ghost-aircraft roll angle, deg
ϕ_{max}	minimum value of maximum angle of bank required during flight along acquiring curve, deg
ψ_{ac}	heading of line AC (fig. A-2), deg
ψ_t	heading of tangent to reference flightpath track at aircraft's position, deg

Derived Constants

$A_{(1)}, A_{(2)}$	constants
$B_{(1)}, B_{(2)}$	constants
B_x, B_y	coordinates of point B in landing-pad system after flightpath select, ft
$C_{(1)}, C_{(2)}$	constants
C_x, C_y	coordinates of point C in landing-pad system, ft
D_a	range at point A, ft
D_{a_1}	range at point A_1 (fig. B-1), ft
D_{b_1}	range at point B_1 (fig. B-1), ft
D_{b_2}	range at point B_2 (fig. B-1), ft
D_c	range at point C (fig. B-1), ft
D_{c_1}	range at point C_1 (fig. B-1), ft
D_{c_2}	range at point C_2 (fig. B-1), ft
D_j	range at point J (fig. B-2), ft
D_{j_1}	range at point J_1 (fig. B-2), ft
D_{j_2}	range at point J_2 (fig. B-2), ft
E	angle subtended by blending curve at center of reference flightpath circle, deg
E_q	value of $\epsilon_q + \Psi_a$ after flightpath select, deg
$\widehat{F}$	nondimensional quantity used in evaluation of $\widehat{\widehat{X}}$
I	indicates right ($I = +1$) or left ($I = -1$) flightpath circle after flightpath select
L	length of acquiring curve measured along x-axis (fig. 6), ft
L_1	distance along acquiring curve, measured along x-axis, where angle of bank changes sign (fig. 6), ft

$L_c^{(i)}$	distances from aircraft to centers of flightpath circles, ft
R_{ll}	nominal radius of flightpath circle after flightpath select, ft
R_{llx}, R_{lly}	coordinates of center of flightpath circle, ft
$\bar{R}_l, \bar{R}_{ll}$	true radius of reference flightpath circle, ft
$R_{l(max)}$	nominal maximum radius of horizontal flightpath circles, ft
$\hat{R}_l$	nondimensional nominal radius of reference flightpath circle
$R_{l(min)x}^{(i)}$	x-coordinates of minimum-radius circles in landing-pad reference frame, ft
$R_{l(min)y}^{(i)}$	y-coordinates of minimum-radius circles in landing-pad reference frame, ft
V_w'	effective wind speed, ft/sec
$\Delta\Psi_f$	heading of final flightpath segment relative to x-axis of landing pad, deg
$\Delta\Psi_l$	angle between line from aircraft to center of reference flightpath circle and x-axis of landing pad, deg
$\Delta\Psi_i$	heading of initial flightpath segment relative to x-axis of landing pad after flightpath select, deg
H_{ri}	aircraft altitude at flightpath select, ft
N_0	angle subtended at center of nominal reference flightpath circle by complete arc of flightpath's circular segment, deg
$\bar{N}_0$	angle subtended at center of true reference flightpath circle by complete arc of flightpath's circular segment, deg
$\hat{\Xi}$	nondimensional coefficient of blending curve
$\hat{X}$	nondimensional ordinate length of entire blending curve
$\hat{\bar{X}}$	nondimensional ordinate length of portion of blending curve lying within arc of nominal flightpath reference circle
Ψ_a	heading of aircraft at flightpath select, deg
Ψ_i	heading of initial, straight flightpath segment, deg
Ψ_{vi}	heading of velocity vector relative to initial, straight flightpath segment at flightpath select, deg

Acronyms

HUD	head-up display
IMC	instrument meteorological conditions
VMC	visual meteorological conditions
VMS	vertical motion simulator
VSRA	V/STOL systems research aircraft

SUMMARY

A piloted simulation test was conducted on the Ames Research Center's vertical motion simulator (VMS) in support of the Phase IIA flight test of NASA's V/STOL systems research aircraft (VSRA). During the simulation several problems were found with the head-up display (HUD) symbol drive laws and the flightpath synthesis. These problems and the solutions devised to solve them are described in this report. Most of the resulting HUD drive-law changes were implemented during the simulation and their effectiveness was verified. Subsequently both the HUD symbol drive-law and flightpath-synthesis changes were implemented in the VSRA and tested successfully in the Phase IIA flight tests.

INTRODUCTION

The Phase IIA flight tests of NASA's VSRA, a YAV-8B Harrier, were performed in late 1991. For the Phase IIA tests, the aircraft was equipped with a programmable HUD, flight computers, and sensors to provide position, velocity, and acceleration data. The aircraft control system used in the tests was a standard, inservice Harrier. The purpose of the flight tests was to evaluate an advanced HUD format, HUD symbol drive laws, and a flightpath-synthesis technique aimed at reducing the visibility minima for landing. The HUD format, shown in figure 1, is described in detail in reference 1. The flightpath-synthesis technique and the HUD symbol drive laws, with the exception of an exponential speed-guidance law, are also described in reference 1. The exponential speed-guidance law is one that is suitable for the type of control system used in the tests; it is described in reference 2. Because the aircraft has a single seat, safety considerations dictated that the flight tests be performed in visual meteorological conditions (VMC). In an attempt to extend the flight test results to instrument meteorological conditions (IMC), a piloted, moving base simulation was conducted on the Ames Research Center's VMS; the visibility conditions were varied from VMC to "zero-zero."

The simulation was conducted just prior to the Phase IIA VSRA flight tests. During the simulation, a variety of problems with the HUD drive laws and flightpath synthesis were uncovered. The purpose of this report is to describe these problems and the changes devised to solve them. Those changes whose implementation required relatively minor code modifications were made and tested during the simulation. All the changes, including those whose implementation required more extensive code modifications, were tested during the flight tests.

The report addresses seven distinct changes to the material contained in references 1 and 2, as follows:

1. A fundamental error in reference 1 is identified and corrected. This error concerns the way in which the flightpath and ghost symbols (fig. 1) were scaled laterally.

2. Pilots noted that, when following the vertical guidance during the deceleration phase after reconfiguration (nozzle drop), the flightpath was invariably below the glide-slope reference (fig. 1). The reason for this vertical error and a correction for it are identified.

3. The speed-guidance law given in reference 2 did not have sufficient flexibility to modify adequately the speed characteristics in the final few hundred feet of range prior to reaching the hover
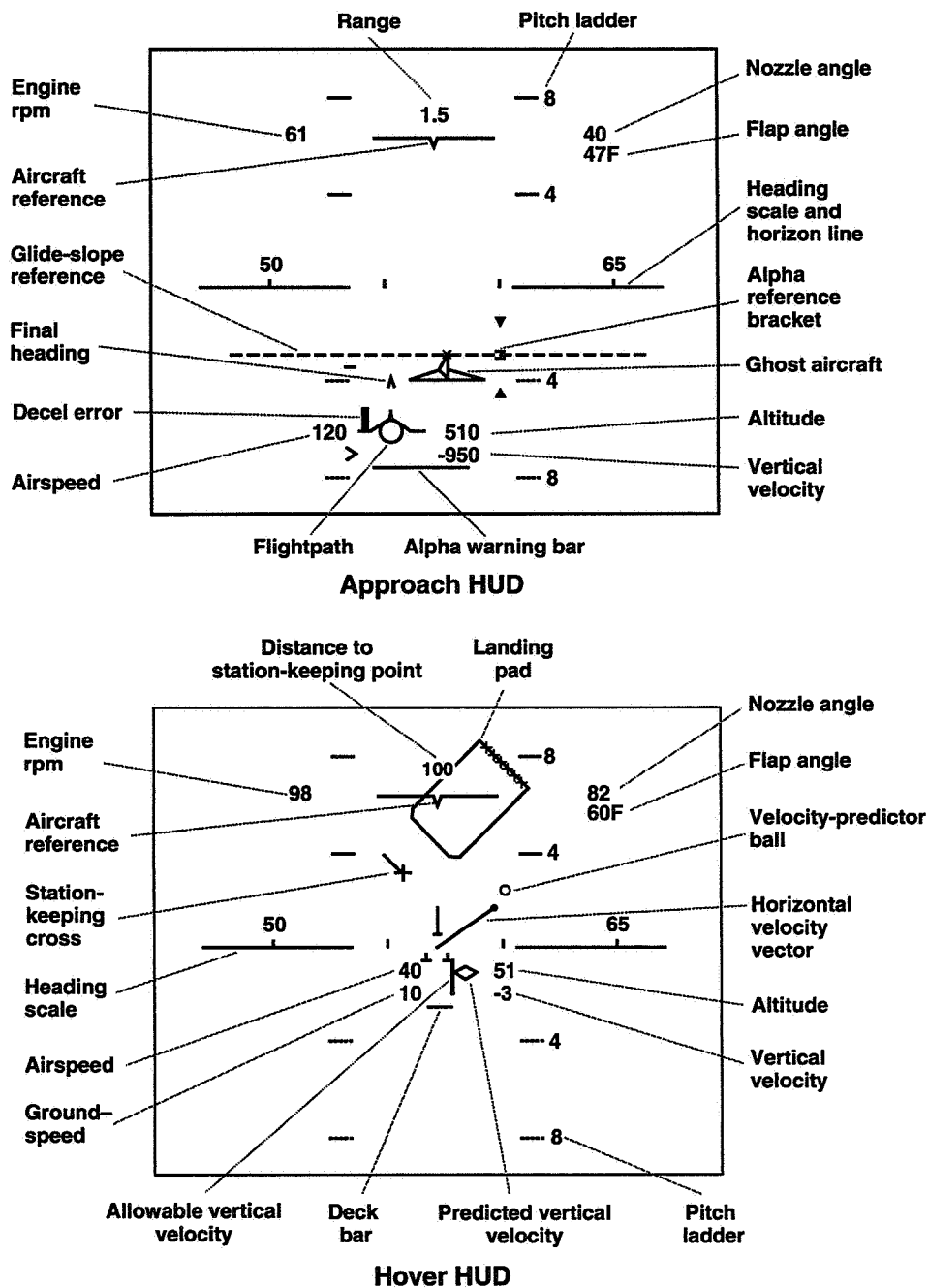
Figure 1. HUD format.

point. This fact became clear when an experienced Harrier pilot requested that the final approach be quickened. The problem is shown to stem from insufficient consideration of the threshold speed and range in the speed-guidance law. An improved speed-guidance law is derived.

4. Recent research (ref. 3) has provided a more rational approach to deriving laws for the velocity-predictor ball (fig. 1) than that used to produce the law given in reference 1. Apart from improved dynamics, this new approach permits a simple means of modifying the ball response independently of

the damping factor and is easier to adjust to pilot requirements. A modified version of the law given in reference 3 is derived to replace that given in reference 1

5. Even when the ghost aircraft was tracked precisely, significant lateral flightpath errors were noted at turn entrances and exits, most notably in the latter. It is shown that this anomaly is caused by discontinuities in the lateral curvature of the reference flightpath at points where straight and circular segments meet. The proposed solution given herein is to remove these discontinuities by providing a "blending curve" in the region where the straight and circular flightpath segments join. This blending curve is designed to provide a reference flightpath with a continuous curvature.

6. It has been noted that if, at the instant of flightpath select, the heading of the aircraft's track differs significantly from that of the reference flightpath, then the required turn to acquire the reference flightpath can be large enough to cause the ghost-aircraft symbol on the HUD to saturate. If, under these circumstances, the pilot is using the HUD for guidance, the ghost gives the direction of the turn but not its magnitude. This lack of information can cause the pilot either to overcontrol or to undercontrol. Overcoming this problem involves defining an "acquiring curve" that provides explicit guidance for the "S" turn to the first straight flightpath segment.

7. In reference 1, no explicit vertical guidance was provided other than a glidepath. The pilot was expected to fly the aircraft until glidepath intercept occurred, as indicated by the descent of the ghost symbol on the HUD. This indication was too abrupt and it resulted in significant glide-slope overshoot. To remedy this problem, the reference flightpath now maintains a constant altitude equal to that of the aircraft at the instant of flightpath select and is gradually blended into the glide slope. This modification is included in the appendixes.

Comprehensive sets of equations for the flightpath synthesis and guidance incorporating the adopted solutions to the problems are given in appendixes A and B. Results of the simulation and flight tests are given in reference 4.

HUD LATERAL SCALING

During the simulation, it was noted by one of the pilots that when performing steady, coordinated turns in calm conditions, both the ghost and flightpath symbols were displaced laterally from the HUD centerline. Although the flightpath tracking task appeared to be satisfactory, it was clear that this lateral displacement should not occur, since it erroneously signified a sideslip. The problem resulted from the manner in which both the flightpath and the ghost symbols were scaled laterally. Lateral scaling is needed because of HUD field-of-view limitations. The HUD projection equipment in the VSRA has a usable lateral field-of-view of about ± 7 deg. Since, at very low speed, in a crosswind, the aircraft yaw relative to the flight direction can easily exceed 20 deg, it is clear that some degree of lateral scaling is needed. In both the simulation and the flight test, the lateral motion of the flightpath and the ghost was reduced to 30% of the full value. In the notation of reference 1, this scaling corresponds to a value of K_ϵ of 0.3. In reference 1, this scaling factor was applied to the lateral motion of both the ghost and the flightpath symbols when defined in Earth-fixed axes prior to the transformation to HUD axes. Clearly, this procedure is in error since the intention was to scale the lateral motion in HUD axes. It follows that the correct approach is to reverse the procedure by applying the transformation first and then applying

3

the lateral scaling factor. The appropriate corrections to the symbol drive laws of reference 1 are to delete the K_ϵ factors from equations (15) and (23), which define the lateral positions of the flightpath and the ghost symbols in Earth-fixed axes, and to multiply by K_ϵ the lateral positions in HUD axes given by equations (17) and (25). These corrections were made for both the VMS simulation and the Phase IIA VSRA flight tests with satisfactory results, at least for the approach task.

Although the new scaling procedure just described is fundamentally sound, further experiments have shown that it results in another problem, noted particularly during large changes of roll angle. In order to see the nature of this problem, consider the path traced out on the HUD by a point fixed in space and far ahead of the aircraft, when the aircraft is rolled at constant pitch angle through 360 deg. Let the azimuth and elevation of the fixed point be M_f and H_f, respectively. The unscaled HUD coordinates of this point, x_f and y_f, are given by

$$x_f = M_f \cos\phi - (H_f - \theta)\sin\phi$$
$$y_f = M_f \sin\phi + (H_f - \theta)\cos\phi$$

where θ and ϕ are the aircraft pitch and roll angles, respectively.

Eliminating ϕ between these equations gives

$$x_f^2 + y_f^2 = M_f^2 + (H_f - \theta)^2$$

from which it follows that, if M_f, H_f, and θ are all constant, the path traced out on the HUD by the fixed point is a circle of radius $\sqrt{M_f^2 + (H_f^2 - \theta^2)}$. Suppose now that the lateral position M_f is scaled by a factor K_ϵ, less than unity, as was done in reference 1. The above equations show that the path of the point is still circular, but of reduced radius $\sqrt{K_\epsilon^2 M_f^2 + (H_f^2 - \theta^2)}$. Alternatively, if the lateral HUD coordinate x_f, rather than M_f, is scaled by K_ϵ, then the path of the point on the HUD is the ellipse

$$x_f^2 K_\epsilon^2 + y_f^2 = M_f^2 + (H_f - \theta)^2$$

oriented so that its major axis is vertical and the ratio of its minor to major axes is K_ϵ.

It follows from the above analysis that, although the method of lateral scaling given in reference 1 produces incorrect angles of sideslip, the path of a fixed point, which could be either the ghost symbol or the flightpath symbol, is at least geometrically similar to that which would be observed if the HUD were unscaled. On the other hand, the new method of scaling, although not showing false sideslip angles, produces a very distorted representation of the path of a fixed point. It turns out that this distortion, although not too noticeable in a precise tracking task where only moderate rates of roll are required, does cause problems in circumstances where large rates of roll and large roll angles are required. The problem occurs because the fixed point appears to move much more vertically than laterally, giving the pilot a strong visual cue that a vertical-control correction is required.

Clearly there is no way to disguise the fact that the lateral motion is being scaled. The scaling will produce an anomaly of one form or another. The best that can be done is to perform the scaling in a way that is the least dangerous. A possible solution is to remove all scaling at speeds high enough that crab angles will not normally exceed the lateral field-of-view of the HUD. The new form of scaling can be introduced at the instant when the terminal guidance is selected, since it is only beyond this point that crab angles can become large.

4

ALTITUDE ERROR DURING APPROACH DECELERATION

As explained in detail in reference 1, the HUD concept used in the VMS simulation and Phase IIA VSRA flight tests employs a ghost aircraft to represent a ficticious aircraft flying ahead of the real aircraft and performing the approach task perfectly. To replicate this desired approach, the pilot maneuvers the real aircraft so that the flightpath symbol (velocity vector) on the HUD is coincident with the ghost aircraft.

During the early phase of the VMS simulation, it was found that during the approach deceleration after reconfiguration (nozzle drop) the aircraft showed a pronounced tendency to fall below the desired flightpath. The maximum altitude error was typically about 30 ft. This altitude error occurred even though the pilot maintained the flightpath symbol precisely on the ghost symbol. The altitude error was qualitatively evident to the pilot since, even though the two symbols were coincident, both were above the glide-slope reference line on the HUD (fig. 1). Surprisingly, this significant inconsistency on the HUD passed unnoticed in the simulation tests of reference 2.

This inconsistency problem was caused by the vertical quickening introduced into the flightpath-symbol vertical-drive law. This quickening was produced by augmenting the vertical velocity with "washed-out" throttle position. The effective vertical velocity used to calculate the vertical position of the flightpath symbol on the HUD (vertical flightpath angle) is given in reference 1 by

$$\widehat{\dot{h}}_c = \dot{h} + \frac{k_{\delta_t} s \delta_t}{s + \sigma_w} \tag{1}$$

where

$\dot{h}$	vertical velocity
$\widehat{\dot{h}}_c$	quickened vertical velocity
δ_t	throttle position
k_{δ_t}	throttle washout gain
s	Laplace transform variable
σ_w	aircraft vertical damping parameter

The reason for using quickened vertical velocity in the flightpath-symbol drive law is to make easier the pilot's task of maintaining the desired flightpath, and it undoubtedly achieves this goal. However, $\widehat{\dot{h}}_c = \dot{h}$ in the long term only if the average deviation of δ_t from some nominal constant is zero in the long term. This condition is met in conventional, constant-speed approaches. In decelerating approaches, the throttle must be advanced continuously to compensate for the gradual loss of aerodynamic lift as the airspeed decreases. In this case, the rate of change of δ_t (i.e., $s\delta_t$ in eq. (1)) is positive for as long as 30 sec, during which time $\widehat{\dot{h}}_c \neq \dot{h}$. This "standoff" error is exaggerated by the long washout time constant $(1/\sigma_w)$ of about 10 sec. Since the HUD flightpath symbol depends on $\widehat{\dot{h}}_c$ rather than $\dot{h}$, it does not provide the pilot with the correct flightpath angle. More specifically, during the deceleration, $\widehat{\dot{h}}_c > \dot{h}$ and the HUD-indicated flightpath angle (measured positive when climbing) is greater than the true flightpath angle by as much as 2 deg. It follows that, if the pilot maintains the flightpath symbol on the ghost, then the true flightpath angle will be less (more negative) than the indicated flightpath angle and the aircraft will settle below the desired flightpath.

To overcome this difficulty, equation (1) was modified to be

$$\widehat{h}_c = \dot{h} + \frac{k_{\delta_t} s(\delta_t - \delta_{tc})}{s + \sigma_w}$$ (2)

where δ_{tc} is the throttle angle required to maintain the desired flightpath angle during the deceleration. In an effort to determine a suitable form for δ_{tc}, a pilot was requested to perform a series of decelerating approaches, in various winds, using the original flightpath-symbol vertical-drive law. The pilot was instructed to use the HUD to keep the ghost on the glide-slope reference line, even though this meant keeping the flightpath and ghost symbols noncoincident. The resulting variation of throttle angle with airspeed are shown in figure 2. It can be seen that the correlation of the data for the various approaches is sufficiently good that the data can be approximated by the single curve of figure 3. This curve was used to define the value of δ_{tc} in equation (2). The modification shown in equation (2) overcame the problem and turned out to be satisfactory over a range of flightpath angles from –2 deg to –5 deg (ref. 4).
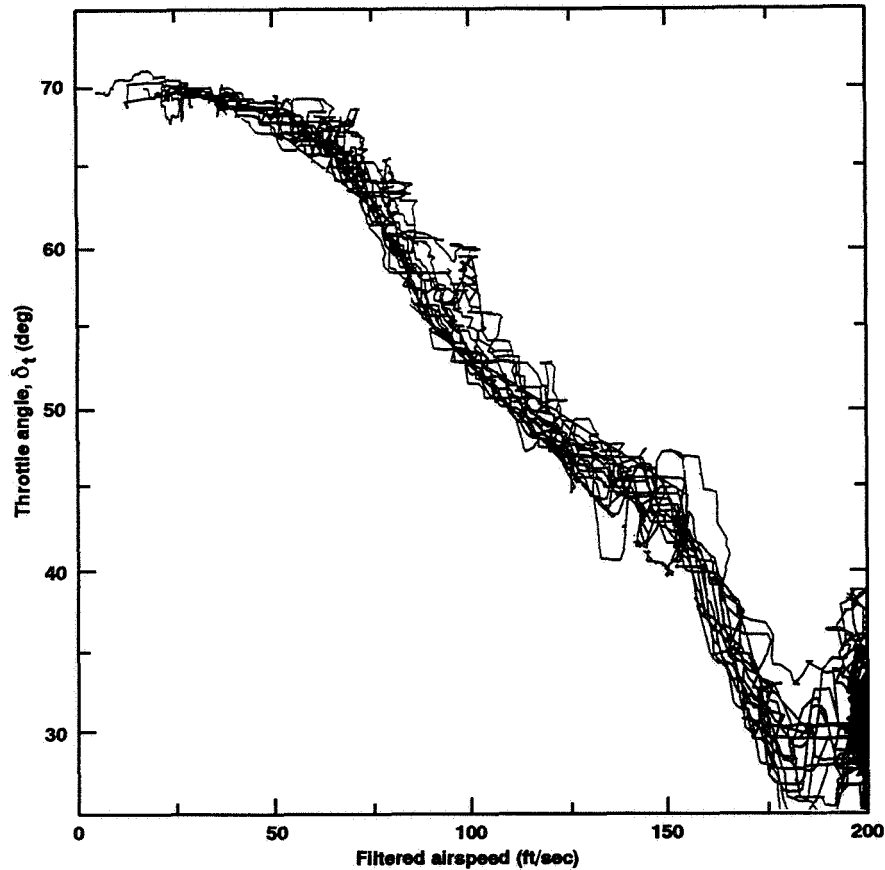

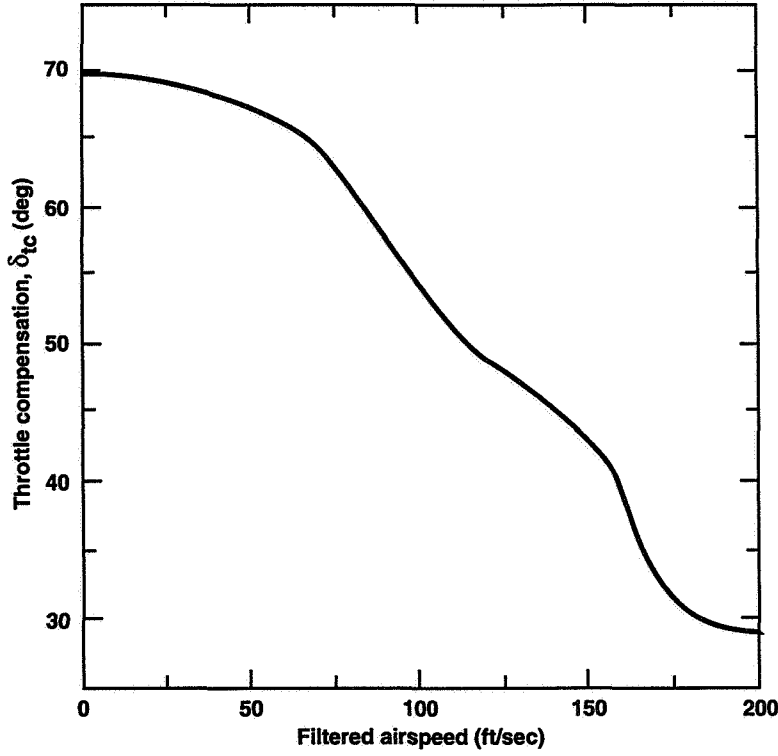Figure 2. Variation of throttle angle with filtered airspeed during deceleration.

6

Figure 3. Throttle compensation used in flightpath-symbol vertical-drive law.

SPEED-GUIDANCE LAW MODIFICATION

The speed-guidance law given in reference 2 consists of two parts. The first part specifies the reconfiguration range, d_r, where the engine nozzle control is moved to the hover position. It is defined to be the range, d, at which the inequality

$$d \leq - \left[v_x - V_{xf} - V'_w \ln\left(\frac{v_x + V'_w}{V_{xf} + V'_w} \right) \right] / \bar{X}_u + D_f \qquad (3)$$

is first satisfied, where

d	aircraft range from the selected station-keeping point
d_r	reconfiguration range
D_f	threshold range
v_x	horizontal longitudinal speed relative to the station-keeping point
V_{xf}	desired value of v_x at the threshold range, D_f
V'_w	effective wind speed (ref. 2)
$\bar{X}_u$	effective value of the sign reversed slope of the speed-versus-range line of the reconfigured aircraft (ref. 2)

The second part of the speed-guidance law specifies that the pilot produce a deceleration, after reconfiguration, given by

$$\dot{v}_{xr} = -\frac{v_x^2}{d} \qquad (4)$$

7

where $\dot{v}_{xr}$ is the reference horizontal longitudinal acceleration.

In the piloted simulation D_f and V_{xf} were initially set at 200 ft and 30 ft/sec, respectively. However, an experienced Harrier pilot, flying in VMC, judged the final approach from the threshold to be too slow. Attempts were made to speed up the final approach to the hover point by changing D_f and V_{xf}, but these changes were unsatisfactory. Changing D_f and V_{xf} changed only the reconfiguration range (eq. (3)), and the guidance law (eq. (4)) always tended to cancel the effect of this change so that the change in the speed of the final approach was only minor. The problem with the overall guidance scheme given above is that the deceleration law is incompatible with the reconfiguration range. The exact deceleration law is given by equation (5) of reference 2, namely

$$\dot{v}_{xr} = \bar{X}_u (v_x + V_w')$$ (5)

where the horizontal longitudinal acceleration $\dot{v}_x$ has been treated as the reference value $\dot{v}_{xr}$.

The problem with this law is that it is strongly dependent on $\bar{X}_u$, which is dependent on the average angle of attack needed during the approach, which, in turn, is dependent on the reconfiguration range. Therefore, unless the pilot moves the engine nozzle to the hover position at precisely the reconfiguration range, the guidance law will not provide guidance to the desired threshold conditions. In essence, equation (5) is not a feedback law and it does not have any continuous acceleration-correction properties. What is required is a version of equation (5) that specifically contains the range d and the threshold parameters D_f and V_{xf}. This version can be achieved by first noting that, during a perfect approach in which the angle of attack is constant and is the correct value, the relationship between speed and range is given by

$$d = -\left[v_x - V_{xf} - V_w' \ln\left(\frac{v_x + V_w'}{V_{xf} + V_w'} \right) \right] / \bar{X}_u + D_f$$ (6)

and this equation may be rearranged to give

$$\bar{X}_u = \frac{-v_x}{d - \left\{ D_f + \left[V_{xf} + V_w' \ln\left(\frac{v_x + V_w'}{V_{xf} + V_w'} \right) \right] / \bar{X}_u \right\}}$$ (7)

which, when substituted into equation (5), gives

$$\dot{v}_x = \frac{-v_x (v_x + V_w')}{d - \left\{ D_f + \left[V_{xf} + V_w' \ln\left(\frac{v_x + V_w'}{V_{xf} + V_w'} \right) \right] / \bar{X}_u \right\}}$$ (8)

Equation (8) is a more exact version of equation (4); it shows clearly that implicit in equation (4) is the assumption that $V_w' = D_f = V_{xf} = 0$. However, the results of both the simulation on the VMS and the simulation reported in reference 2 indicate that, when equation (4) is used for speed guidance, nonzero values of V_w' were compensated for quite well. Therefore, it is reasonable to presume that the same situation would be true if equation (8) were used for speed guidance. Setting $V_w' = 0$ in equation (8) gives

$$\dot{v}_{xr} = \frac{-v_x^2}{d - \left(D_f + \frac{V_{xf}}{\bar{X}_u} \right)}$$ (9)

8

This equation is the guidance law that emerged from the VMS simulation as being satisfactory (ref. 4). Although it depends on $\bar{X}_u$, the dependency is not so strong that the speed guidance is significantly affected by errors in the reconfiguration range.

VELOCITY-PREDICTOR-BALL LAW

The velocity-predictor-ball law used in the VMS simulation and Phase IIA VSRA flight tests differed somewhat from that given in reference 1. In reference 1 the commanded horizontal velocities $\hat{v}_{xc}$ and $\hat{v}_{yc}$ are given by the expressions

$$\hat{v}_{xc} = v_x + T_{\dot{v}}\hat{\dot{v}}_x - \frac{K_{\delta_x}T_2 s \delta_x}{T_2 s + 1} \tag{10}$$

$$\hat{v}_{yc} = v_y + T_{\dot{v}}\hat{\dot{v}}_y + \frac{K_{\delta_y}T_2 s \delta_y}{T_2 s + 1} \tag{11}$$

where

$\hat{v}_{xc}, \hat{v}_{yc}$	commanded horizontal translational velocities
v_x, v_y	horizontal translational speeds
$\hat{\dot{v}}_x, \hat{\dot{v}}_y$	smoothed estimates of the horizontal translational accelerations
δ_x, δ_y	longitudinal and lateral pilot control inputs
$K_{\delta_x}, K_{\delta_y}$	control-input gains
T_2	control-input washout time constant
$T_{\dot{v}}$	horizontal-tracking time constant

This law was deduced in an ad hoc manner with the gains $K_{\delta_x}, K_{\delta_y}, T_2$, and $T_{\dot{v}}$ set, experimentally, in piloted simulations.

A more rationally designed predictor-ball law was derived in reference 3 and tested on a variable-stability helicopter. One of the attractive features of this law is that its principal dynamic characteristic (break frequency) can be varied through a single frequency parameter, Ω_0, while maintaining a closed-loop, third-order, binomial transfer function for the horizontal velocity response to a commanded predictor-ball position. Since all the gains are functions of Ω_0, it is easy to change the speed of response of the aircraft to a given commanded ball position. A variation of the approach used in reference 3 was used in the VMS simulation and Phase IIA VSRA flight tests. The third-order, binomial transfer function was chosen to represent the response of the aircraft horizontal position rather than the horizontal velocity. The steps in the derivation of the corresponding predictor-ball law closely follow those outlined in reference 3. The resulting law is

$$\hat{v}_{xc} = v_x + \frac{2}{\Omega_0}\hat{\dot{v}}_x - \frac{gD_x C_{\dot{\theta}} s(s + 4\Omega_0)\delta_x}{4\Omega_0{}^3(s + \sigma_x)(s + D_x)} \tag{12}$$

$$\hat{v}_{yc} = v_y + \frac{2}{\Omega_0}\hat{\dot{v}}_y + \frac{gD_y C_{\dot{\phi}} s(s + 4\Omega_0)\delta_y}{4\Omega_0{}^3(s + \sigma_y)(s + D_y)} \tag{13}$$

9

where

Ω_0	translational velocity response frequency
g	acceleration due to gravity
D_x, D_y	aircraft pitch and roll damping constants
$C_{\dot\theta}, C_{\dot\phi}$	pitch and roll rate sensitivity to pilot control inputs
σ_x, σ_y	aircraft horizontal translational damping constants

AIRCRAFT/GHOST FLIGHTPATH GEOMETRY

The kinematical implications of a flightpath guidance technique that uses a ghost aircraft flying ahead of the real aircraft should be examined before we consider a method of reducing flightpath errors at turn entrances and exits (problem number 5 in the Introduction). Consider the situation depicted in figure 4. The real aircraft is being maintained on a predetermined flightpath (solid line) such that its velocity vector always points to a ghost aircraft located on an adjacent flightpath (dashed line). Let the flightpath of the aircraft be given by

$$\mathbf{r}_a = \mathbf{r}_a(d) \tag{14}$$

where $\mathbf{r}_a$ is the vector position of the real aircraft measured from an origin 0 and d is the aircraft's range measured from a fixed point A on the flightpath (fig. 4). The unit tangent vector to the aircraft's flightpath at the position of the aircraft is $\mathbf{r}'_a$, where the prime denotes differentiation with respect to the range, d. It follows from the geometry of figure 4 that the position of the ghost aircraft, $\mathbf{r}_g$, is given by

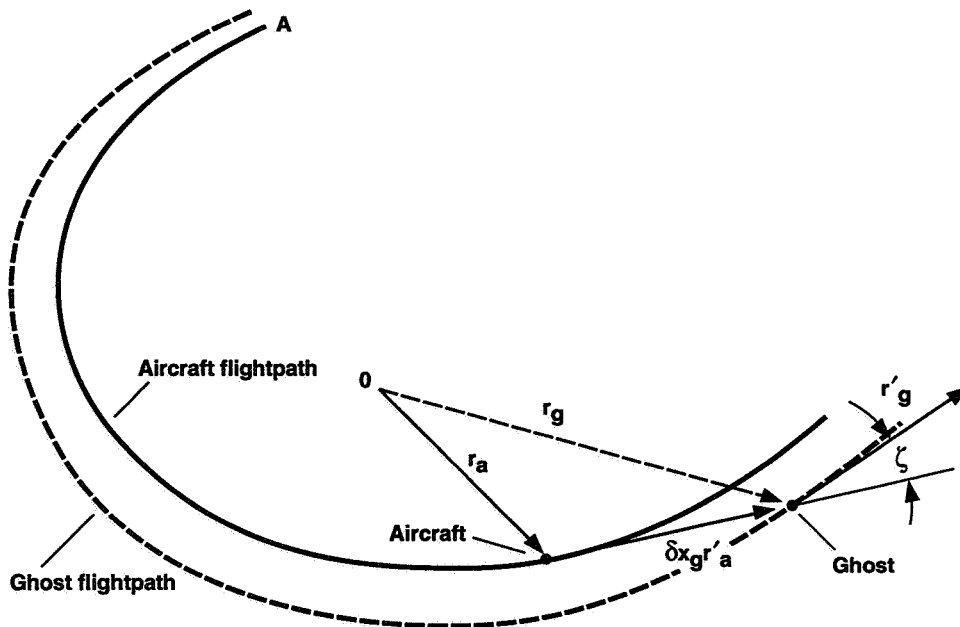$$\mathbf{r}_g = \mathbf{r}_a + \delta x_g \mathbf{r}'_a \tag{15}$$

Figure 4. Aircraft/ghost flightpath geometry.

10

where δx_g is the distance from the ghost aircraft to the real aircraft. The unit tangent vector to the ghost aircraft's flightpath, $\mathbf{r}'_g$, is obtained by differentiating equation (15) with respect to d; thus,

$$\mathbf{r}'_g = \mathbf{r}'_a + \delta x_g \mathbf{r}''_a + \delta x'_g \mathbf{r}'_a \tag{16}$$

The direction of the ghost aircraft relative to the real aircraft, ζ (fig. 4), is given by the inner product of $\mathbf{r}'_g$ and $\mathbf{r}'_a$, as follows,

$$\mathbf{r}'_g \cdot \mathbf{r}'_a = |\mathbf{r}'_g||\mathbf{r}'_a| \cos \zeta = (\mathbf{r}'_a + \delta x_g \mathbf{r}''_a + \delta x'_g \mathbf{r}'_a) \cdot \mathbf{r}'_a \tag{17}$$

Since $\mathbf{r}'_a$ is a unit vector,

$$\mathbf{r}'_a \cdot \mathbf{r}'_a = |\mathbf{r}'_a|^2 = 1 \tag{18}$$

Differentiating equation (18) with respect to d results in

$$\mathbf{r}'_a \cdot \mathbf{r}''_a = 0 \tag{19}$$

Applying equations (18) and (19) to equation (17) shows that

$$|\mathbf{r}'_g| \cos \zeta = 1 + \delta x'_g \tag{20}$$

But it follows from equation (16), with equations (18) and (19), that

$$|\mathbf{r}'_g|^2 = [\mathbf{r}'_a(1 + \delta x'_g) + \delta x_g \mathbf{r}''_a] \, [\mathbf{r}'_a(1 + \delta x'_g) + \delta x_g \mathbf{r}''_a]$$

$$= \mathbf{r}'_a \cdot \mathbf{r}'_a (1 + \delta x'_g)^2 + \delta x_g{}^2 \mathbf{r}''_a \cdot \mathbf{r}''_a + 2\delta x_g(1 + \delta x'_g)\mathbf{r}'_a \cdot \mathbf{r}''_a$$

$$= (1 + \delta x'_g)^2 + \left(\frac{\delta x_g}{\rho}\right)^2 \tag{21}$$

where ρ is the radius of curvature of the real aircraft's flightpath at the position of the aircraft. Specifically,

$$\rho \overset{\text{def}}{=} \frac{1}{\sqrt{\mathbf{r}''_a \cdot \mathbf{r}''_a}} \tag{22}$$

It follows from equations (20) and (21) that

$$\cos \zeta = \frac{1}{\sqrt{1 + \left[\frac{\delta x_g}{(1+\delta x'_g)\rho}\right]^2}} \tag{23}$$

The term $\delta x'_g$ expressed as a function of the aircraft's kinematical variables is:

$$\delta x'_g = \frac{d\delta x_g}{dd} = \frac{d\delta x_g}{dt}\frac{dt}{dd} = \frac{\delta \dot{x}_g}{v_t} \tag{24}$$

where v_t is the groundspeed of the real aircraft. If, as is usual, the ghost lead distance δx_g is made proportional to v_t, that is,

$$\delta x_g = v_t \Delta T_g \tag{25}$$

11

where ΔT_g is the (constant) ghost lead time, then differentiating equation (25) with respect to time and substituting for $\delta \dot{x}_g$ in equation (24) gives the following final expression for $\delta x'_g$:

$$\delta x'_g = \frac{\dot{v}_t \Delta T_g}{v_t} \tag{26}$$

where $\dot{v}_t$ is the aircraft's acceleration along the ground track.

It is instructive to evaluate the implications of equations (23) and (26) by means of two examples.

Example 1

An aircraft, traveling at a constant groundspeed, v_t, of 200 ft/sec ($\dot{v}_t = 0$) on a circular flightpath of radius, ρ, of 4,000 ft, is just about to turn onto a straight flightpath segment ($\rho = \infty$). The lead time of the ghost aircraft, ΔT_g, is 10 sec. It follows from equation (25) that the lead distance of the ghost aircraft, δx_g, is 2,000 ft and from equation (24) that $\delta x'_g = 0$. Just prior to and just after exiting the turn, $\zeta = 26.6$ deg and $\zeta = 0$ deg, respectively (eq. (23)). Therefore, in exiting the turn, the ghost-aircraft flightpath instantly changes direction by 26.6 deg relative to the real-aircraft flightpath. The pilot perceives a sudden change of direction of this magnitude as an undesirable heading transient despite the measure taken in reference 1 to smooth it out by introducing a turn-exit blend distance.

Example 2.

As in example 1, the aircraft is traveling at a constant groundspeed, v_t, of 200 ft/sec ($\dot{v}_t = 0$) on a circular flightpath of radius, ρ, of 4,000 ft and a ghost-aircraft lead time, ΔT_g, of 10 sec. However, in this example, the aircraft is suddenly decelerated at 8 ft/sec ($\dot{v}_t = -8$ ft/sec) while still turning. A deceleration of this magnitude is produced on a Harrier, typically, when the engine nozzle is moved to the hover position. At the instant of deceleration, the value of $\delta x'_g$ changes from zero to -0.4 (eq. (24)) and the measure of ζ changes from 26.6 deg to 39.8 deg (eq. (23)). This 13.2-deg change of ζ is probably not discernible to the pilot. However, if future flightpath requirements are for smaller radii circles to be flown very accurately, then the effect could become more important. If, for example, the radius were to be 2,000 ft instead of 4,000 ft, then the change of ζ would be a much more significant 32.4 deg.

BLENDING-CURVE GEOMETRY

The previous analysis of the aircraft/ghost flightpath geometry indicates that it is desirable to have a synthesized flightpath with continuous curvature. One way to achieve this continuity, while retaining much of the synthesis technique of reference 1, is developed in this section.

The initial process of synthesizing a flightpath trajectory involves connecting initial and final straight segments by a circular segment with a given nominal radius, R_l. This procedure produces a flightpath whose curvature is continuous except at the two points of tangency of the straight and circular segments. The point of tangency of one of the straight segments and the circle is shown in figure 5 at point 2. The approach adopted here to remove the curvature discontinuity is to modify the geometry of the flightpath locally by means of a "blending curve." The process of adding a blending curve between the straight and circular segments starts by defining a second circular segment with the same center as the original but of slightly smaller radius, $\bar{R}_l$, and connecting this new circular segment and the straight segment with
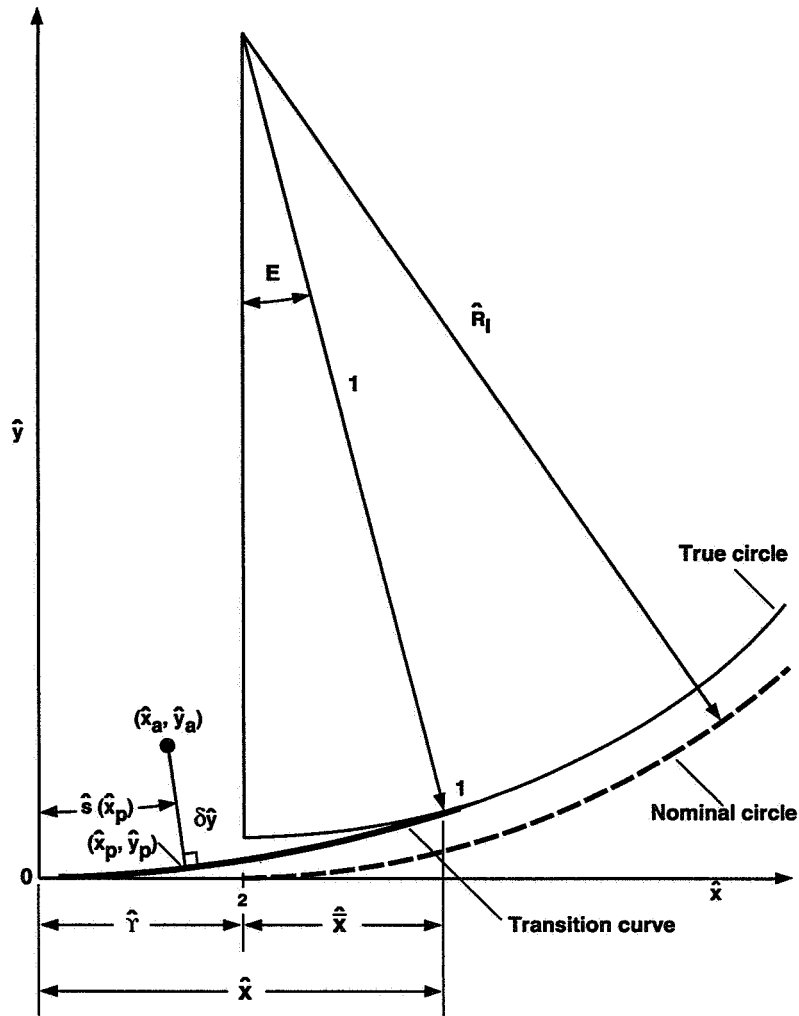
12

Figure 5. Flightpath transition-curve geometry.

a cubic blending curve, 01 (fig. 5). This blending curve is defined to have, at point 0, the same slope and zero curvature as the straight segment and, at point 1, the same slope and curvature as the circle. Since the blending curve is a cubic, its curvature is approximately linear along its length, varying from zero at point 0 to $1/\bar{R}_l$ at point 1. The complete synthesized flightpath consists of a straight segment, a blending curve, a circle of radius $\bar{R}_l$, a second blending curve, and a final straight segment. All the dimensions in figure 5 have been normalized by the radius $\bar{R}_l$ so that the true flightpath circle has unit radius. Normalization is uniformly indicated by a hat over the symbol.

The blending curve has the form

$$\hat{y} = \hat{\Xi}\hat{x}^3 \tag{27}$$

As shown in figure 5, the origin of the blending curve is defined to be at a normalized distance $\hat{\Upsilon}$ from the intersection of the straight segment and the nominal flightpath circle (point 2 of fig. 5). Equation (27) satisfies the required conditions of continuity, slope, and curvature at point 0. The task now is to determine the value of $\hat{\Xi}$ consistent with the required continuity, slope, and curvature at point 1.

The equation of the true flightpath circle in the coordinate system shown in figure 5 is

$$(\hat{x} - \hat{\Upsilon})^2 + (\hat{y} - \hat{R}_l)^2 \tag{28}$$

The following relationships express the required continuity of position, slope, and curvature (second derivative) at point 1·

$$\text{position} \qquad (\hat{X} - \hat{\Upsilon})^2 + (\hat{\Xi}\hat{X}^3 - \hat{R}_l)^2 = 1 \tag{29}$$

$$\text{slope} \qquad 3\hat{\Xi}\hat{X}^2 = -\left(\frac{\hat{X} - \hat{\Upsilon}}{\hat{\Xi}\hat{X}^3 - \hat{R}_l}\right) \tag{30}$$

$$\text{curvature} \qquad 6\hat{\Xi}\hat{X} = -\left[\frac{1 + \left(\frac{\hat{X}-\hat{\Upsilon}}{\hat{\Xi}\hat{X}^3-\hat{R}_l}\right)^2}{\hat{\Xi}\hat{X}^3 - \hat{R}_l}\right] \tag{31}$$

From equations (30) and (31),

$$\frac{2}{\hat{X}} = \frac{1 + \left(\frac{\hat{X}-\hat{\Upsilon}}{\hat{\Xi}\hat{X}^3-\hat{R}_l}\right)^2}{\hat{X} - \hat{\Upsilon}} \tag{32}$$

Substituting for $(\hat{\Xi}\hat{X}^3 - \hat{R}_l)^2$ from equation (29) into equation (30) and simplifying gives the following cubic equation:

$$\widehat{\overline{X}}^3 - \frac{\widehat{\overline{X}}}{2} + \frac{\hat{\Upsilon}}{2} = 0 \tag{33}$$

where the quantity $\widehat{\overline{X}}$ is defined as

$$\widehat{\overline{X}} \overset{\text{def}}{=} \hat{X} - \hat{\Upsilon} \tag{34}$$

The appropriate real, positive solution of equation (33) is

$$\widehat{\overline{X}} = \sqrt{\frac{2}{3}}\cos\left(\frac{\hat{F} + 4\pi}{3}\right) \tag{35}$$

where the quantity $\hat{F}$ is defined as

$$\hat{F} \overset{\text{def}}{=} \arccos\left(-\hat{\Upsilon}\sqrt{\frac{27}{2}}\right) \qquad \frac{\pi}{2} \leq \hat{F} \leq \pi \tag{36}$$

It follows from equation (36) that

$$\hat{\Upsilon}\sqrt{\frac{27}{2}} \leq 1 \tag{37}$$

or

$$\hat{\Upsilon} \leq \sqrt{\frac{2}{27}} = 0.272166 \tag{38}$$

14

and from equation (35) that

$$\widehat{X} \leq \sqrt{\frac{2}{3}}\cos\left(\frac{5\pi}{3}\right) = 0.408248 \tag{39}$$

These restrictions on the value of $\widehat{\Upsilon}$ and $\widehat{X}$ should cause no difficulties for most applications.

The value of $\widehat{\Xi}$ is obtained by eliminating the expression $(\widehat{\Xi}\widehat{X}^3 - \widehat{R}_l)$ between equations (29) and (30), giving

$$\widehat{\Xi} = \frac{\widehat{X}}{3\widehat{X}^2\sqrt{1 - \widehat{X}^2}} \tag{40}$$

and from equation (29), $\widehat{R}_l$ is found to be given by

$$\widehat{R}_l = \widehat{\Xi}\widehat{X}^3 + \sqrt{1 - \widehat{X}^2} \tag{41}$$

The blending curve is defined uniquely by the quantity $\widehat{\Upsilon}$ Given $\widehat{\Upsilon}$, the value of $\widehat{X}$ is given by equations (35) and (36) and the values of $\widehat{\Xi}$ and $\widehat{R}_l$ are given by equations (40) and (41), respectively.

If the aircraft is in the flightpath segment defined by the blending curve, then the distance $\hat{s}(\hat{x}_p)$ along the blending curve from the point 0 (fig. 5) to the foot of the perpendicular $(\hat{x}_p, \hat{y}_p)$ and the perpendicular distance $\delta\hat{y}$ (fig. 5) must be determined. These distances are needed to determine the range and lateral deviation of the aircraft for guidance purposes.

The equation of a line from the aircraft $(\hat{x}_a, \hat{y}_a)$ perpendicular to the blending curve, $\hat{y} = \widehat{\Xi}\hat{x}^3$, is given by

$$\hat{y} - \hat{y}_a = \frac{-1}{3\widehat{\Xi}\hat{x}^2}(\hat{x} - \hat{x}_a) \tag{42}$$

and, therefore, the coordinate $\hat{x}_p$ at the intersection of this perpendicular and the blending curve is given by

$$\widehat{\Xi}\hat{x}_p^3 - \hat{y}_a = \frac{-1}{3\widehat{\Xi}\hat{x}_p^2}(\hat{x}_p - \hat{x}_a)$$

or

$$3\widehat{\Xi}^2\hat{x}_p^5 - 3\widehat{\Xi}\hat{y}_a\hat{x}_p^2 + \hat{x}_p - \hat{x}_a = 0 \tag{43}$$

An approximate solution of equation (43) may be obtained by setting $\hat{x}_p = \hat{x}_a + \hat{\imath}$, substituting this expression for $\hat{x}_p$ in equation (43), and neglecting powers of $\hat{\imath}$ greater than one. After simplification, the result is

$$\hat{\imath} = \frac{3\widehat{\Xi}\hat{x}_a^2(\hat{y}_a - \widehat{\Xi}\hat{x}_a^3)}{1 - 3\widehat{\Xi}\hat{x}_a(2\hat{y}_a - 5\widehat{\Xi}\hat{x}_a^3)} \tag{44}$$

The coordinate $\hat{y}_p$ is given by

$$\hat{y}_p = \widehat{\Xi}\hat{x}_p^3 \tag{45}$$

15

and the normalized perpendicular distance from the aircraft to the blending curve, or lateral deviation, $\delta\hat{y}$, is given by

$$\delta\hat{y} = \sqrt{(\hat{x}_p - \hat{y}_a)^2 + (\hat{y}_p - \hat{y}_a)^2} \qquad (46)$$

The normalized distance $\hat{s}(\hat{x})$ along the blending curve is obtained from the differential equation

$$\frac{d\hat{s}(\hat{x})}{d\hat{x}} = \sqrt{1 + \left(\frac{d\hat{y}}{d\hat{x}}\right)^2} \qquad (47)$$

where $\hat{y} = \widehat{\Xi}\hat{x}^3$. The formal solution of equation (47) is

$$\hat{s}(\hat{x}_p) = \int_0^{\hat{x}_p} (1 + 9\widehat{\Xi}^2\hat{x}^4)^{1/2} d\hat{x} \qquad (48)$$

This integral cannot be evaluated in terms of the standard elementary functions; an approximate evaluation can be obtained by expressing the integrand in the power series

$$(1 + 9\widehat{\Xi}^2\hat{x}^4)^{1/2} = 1 + \frac{9}{2}\widehat{\Xi}^2\hat{x}^4 - \frac{81}{8}\widehat{\Xi}^4\hat{x}^8 + \qquad (49)$$

which converges provided

$$9\widehat{\Xi}^2\hat{x}^4 < 1 \qquad (50)$$

The largest value of $\hat{x}$ along the blending curve is $\widehat{X}$. Therefore, the limiting value of $\widehat{X}$ for which the power series expansion converges is given by (eq. 40))

$$9\widehat{\Xi}^2\widehat{X}^4 = \frac{\widehat{X}^2}{1 - \widehat{X}^2} < 1 \qquad (51)$$

or

$$\widehat{X} < \frac{1}{\sqrt{2}} = 0.707107 \qquad (52)$$

Since the solution of equation (33) is valid only for $\widehat{X} \leq 0.408248$, it follows that the power series expansion converges for the solutions of interest.

Substituting equation (49) into equation (48) and performing the integrations gives

$$\hat{s}(\hat{x}_p) = \hat{x}_p + \frac{9}{10}\widehat{\Xi}^2 x_p^5 - \frac{9}{8}\widehat{\Xi}^4\hat{x}_p^9 + \qquad (53)$$

The maximum value of $\hat{s}(\hat{x}_p)$ occurs when $\hat{x}_p = \widehat{X}$. Using the first three terms of the series gives

$$\hat{s}(\widehat{X}) \approx \widehat{X}(1 + \frac{9}{10}\widehat{\Xi}^2\widehat{X}^4 - \frac{9}{8}\widehat{\Xi}^4\widehat{X}^8) \qquad (54)$$

16

and substituting for $\hat{\Xi}$ from equation (40) gives

$$\hat{s}(\widehat{X}) \approx \widehat{X}\left[1 + \frac{1}{10}\left(\frac{\widehat{\widehat{X}}^2}{1 - \widehat{\widehat{X}}^2}\right) - \frac{1}{72}\left(\frac{\widehat{\widehat{X}}^2}{1 - \widehat{\widehat{X}}^2}\right)^2\right] \tag{55}$$

Since the largest value of $\widehat{\widehat{X}}$ is 0.408248, and the corresponding value of $\widehat{X}$ is 0.680414, it follows from equation (55) that the the largest value of $\hat{s}(\hat{x}_p)$ is 0.693643. The corresponding value obtained from equation (48) (with $\hat{x}_p = 0.408248$) by numerical integration is 0.693668. Therefore, the error in using the first three terms of equation (53) is always less than 0.000025. For a nominal turn radius of 4,000 ft, the distance error is always less than 0.1 ft.

ACQUIRING CURVE

The purpose of the "acquiring curve" is to provide a smooth capture of the initial straight segment of the synthesized flightpath so that the pilot is relieved of the task of precisely aligning the heading of the aircraft's velocity vector with that of the initial straight segment. By appending such a curve, the flightpath symbol on the HUD is made coincident with the ghost-aircraft symbol immediately at guidance select, and lateral guidance along the acquiring curve is provided through the ghost symbol to remove any initial misalignment between the velocity vector and the initial, straight flightpath segment.

The first task in providing an acquiring curve and in determining those properties of it needed to drive the ghost symbol is to choose an appropriate analytical form. This form must be capable of representing a flightpath similar to one that the pilot himself would use in correcting the heading of the velocity vector; it must also be analytically tractable. Of the many reasonable possibilities, the one selected herein is a two-segment sine function to represent the second derivative of the acquiring curve (fig. 6). The rationale for this choice is based on the observation that, in correcting for a velocity-vector misalignment, the pilot would need to roll the aircraft toward the required flightpath track to produce a lateral acceleration relative to the track and then to roll in the reverse direction to reverse the lateral acceleration until the lateral velocity relative to the track is zero ("S" turn maneuver). It follows that, since the path curvature is proportional to lateral acceleration and since path curvature is approximately equal to the second derivative of the path, the form shown in figure 6 is a reasonable representation of what the second derivative of the path would look like if the pilot himself were to perform the misaligment correction task. A second important consideration in the selection of the form of the acquiring curve is that the curvature should be continuous as required to avoid discontinuities in the angle between the directions of flight of the ghost aircraft and the real aircraft.

The equations for the form of the second derivative of the acquiring curve along with the first and second integrals, giving the slope and ordinate, are

Segment 1 $\quad 0 \leq x < L_1$

$$\left(\frac{d^2y}{dx^2}\right)_1 = A_{(1)} \sin \pi\left(\frac{x}{L_1}\right) \tag{56}$$

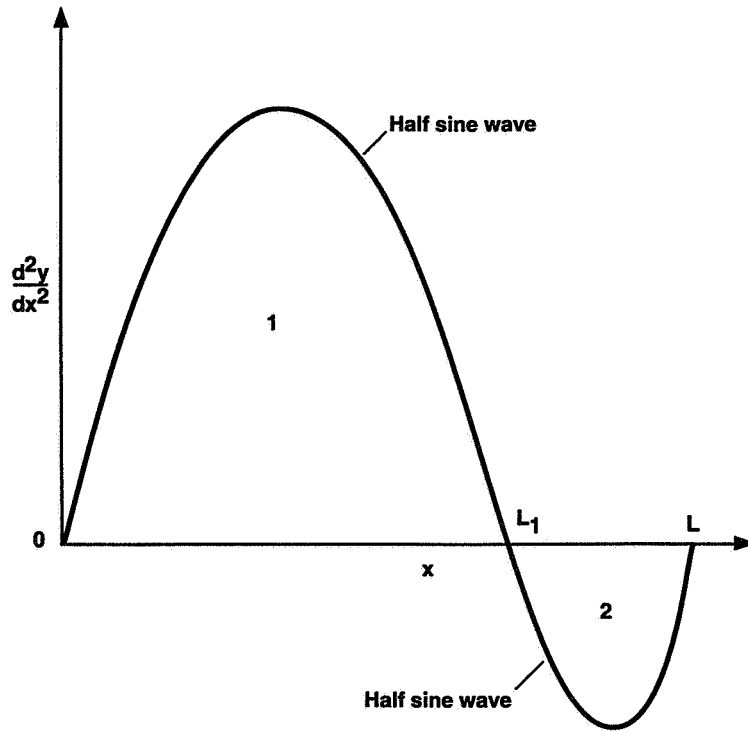$$\left(\frac{dy}{dx}\right)_1 = -\frac{A_{(1)}L_1}{\pi} \cos \pi\left(\frac{x}{L_1}\right) + B_{(1)} \tag{57}$$

Figure 6. Acquiring-curve geometry.

$$(y)_1 = -\frac{A_{(1)}L_1^2}{\pi^2}\sin\pi\left(\frac{x}{L_1}\right) + B_{(1)}x + C_{(1)} \tag{58}$$

Segment 2 $L_1 \leq x \leq L$

$$\left(\frac{d^2y}{dx^2}\right)_2 = A_{(2)}\sin\pi\left(\frac{x - L_1}{L - L_1}\right) \tag{59}$$

$$\left(\frac{dy}{dx}\right)_2 = -A_{(2)}\left(\frac{L - L_1}{\pi}\right)\cos\pi\left(\frac{x - L_1}{L - L_1}\right) + B_{(2)} \tag{60}$$

$$(y)_2 = -A_{(2)}\left(\frac{L - L_1}{\pi}\right)^2\sin\pi\left(\frac{x - L_1}{L - L_1}\right) + B_{(2)}x + C_{(2)} \tag{61}$$

where

L length of the acquiring curve measured along the x-axis (fig. 6)

L_1 distance along the acquiring curve, measured along the x-axis, where the angle of bank changes sign (fig. 6)

$A_{(1)}, A_{(2)}$ constants

$B_{(1)}, B_{(2)}$ constants

$C_{(1)}, C_{(2)}$ constants

18

The six constants $A_{(1)}, A_{(2)}, B_{(1)}, B_{(2)}, C_{(1)},$ and $C_{(2)}$ are set by the boundary conditions

$$\left(\frac{dy}{dx}\right)_{1(x=0)} = E_q - \Psi_i \tag{62}$$

$$\left(\frac{dy}{dx}\right)_{2(x=L)} = 0 \tag{63}$$

$$\left(\frac{dy}{dx}\right)_{1(x=L_1)} = \left(\frac{dy}{dx}\right)_{2(x=L_1)} \tag{64}$$

$$(y)_{1(x=0)} = 0 \tag{65}$$

$$(y)_{1(x=L_1)} = (y)_{2(x=L_1)} \tag{66}$$

$$(y)_{2(x=L)} = 0 \tag{67}$$

where

E_q heading of the HUD flightpath symbol at flightpath select

Ψ_i heading of the initial flightpath segment

Substituting the slopes and ordinates from equations (57), (58), (60), and (61) into equations (62)–(67) gives the following linear matrix equation whose solution vector contains the integration constants

$$\begin{pmatrix} -\frac{L_1}{\pi} & 0 & 1 & 0 & 0 & 0 \\ \frac{L_1}{\pi} & \frac{(L-L_1)}{\pi} & 1 & -1 & 0 & 0 \\ 0 & \frac{(L-L_1)}{\pi} & 0 & 1 & 0 & 0 \\ 0 & 0 & L_1 & -L_1 & 0 & 1 \\ 0 & 0 & 0 & L & 0 & 1 \\ 0 & 0 & 0 & 0 & 1 & 0 \end{pmatrix} \begin{pmatrix} A_{(1)} \\ A_{(2)} \\ B_{(1)} \\ B_{(2)} \\ C_{(1)} \\ C_{(2)} \end{pmatrix} = \begin{pmatrix} E_q - \Psi_i \\ 0 \\ 0 \\ 0 \\ 0 \\ 0 \end{pmatrix} \tag{68}$$

The solution of equation (68) is

$$\begin{pmatrix} A_{(1)} \\ A_{(2)} \\ B_{(1)} \\ B_{(2)} \\ C_{(1)} \\ C_{(2)} \end{pmatrix} = \begin{pmatrix} -\frac{(E_q-\Psi_i)\pi(L+L_1)}{2L_1 L} \\[2mm] \frac{(E_q-\Psi_i)\pi L_1}{2L(L-L_1)} \\[2mm] \frac{(E_q-\Psi_i)(L-L_1)}{2L} \\[2mm] -\frac{(E_q-\Psi_i)L_1}{2L} \\[2mm] 0 \\[2mm] \frac{(E_q-\Psi_i)L_1}{2} \end{pmatrix} \tag{69}$$

Substituting the values of $A_{(1)}, A_{(2)}, B_{(1)}, B_{(2)}, C_{(1)},$ and $C_{(2)}$ from equation (69) into equations (56)–(61) and expressing the result in terms of the nondimensional variables

19

$$\hat{x} = \frac{x}{L} \qquad \hat{y} = \frac{y}{L} \qquad \hat{L}_1 = \frac{L_1}{L}$$

gives the final equations for the acquiring curve and its first and second derivatives:

Segment 1 $\quad 0 \le \hat{x} < \hat{L}_1$

$$\left(\frac{d^2\hat{y}}{d\hat{x}^2}\right)_1 = -\frac{(E_q - \Psi_i)\pi(1 + \hat{L}_1)}{2\hat{L}_1} \sin \pi\left(\frac{\hat{x}}{\hat{L}_1}\right) \tag{70}$$

$$\left(\frac{d\hat{y}}{d\hat{x}}\right)_1 = \frac{(E_q - \Psi_i)}{2}\left[(1 + \hat{L}_1)\cos \pi\left(\frac{\hat{x}}{\hat{L}_1}\right) + (1 - \hat{L}_1)\right] \tag{71}$$

$$(\hat{y})_1 = \frac{(E_q - \Psi_i)}{2}\left[\frac{\hat{L}_1(1 + \hat{L}_1)}{\pi} \sin \pi\left(\frac{\hat{x}}{\hat{L}_1}\right) + (1 - \hat{L}_1)\hat{x}\right] \tag{72}$$

Segment 2 $\quad \hat{L}_1 \le \hat{x} \le 1$

$$\left(\frac{d^2\hat{y}}{d\hat{x}^2}\right)_2 = \frac{(E_q - \Psi_i)\pi\hat{L}_1}{2(1 - \hat{L}_1)} \sin \pi\left(\frac{\hat{x} - \hat{L}_1}{1 - \hat{L}_1}\right) \tag{73}$$

$$\left(\frac{d\hat{y}}{d\hat{x}}\right)_2 = -\frac{(E_q - \Psi_i)}{2}\left[\hat{L}_1 \cos \pi\left(\frac{\hat{x} - \hat{L}_1}{1 - \hat{L}_1}\right) + \hat{L}_1\right] \tag{74}$$

$$(\hat{y})_2 = -\frac{(E_q - \Psi_i)}{2}\left[\frac{\hat{L}_1(1 - \hat{L}_1)}{\pi} \sin \pi\left(\frac{\hat{x} - \hat{L}_1}{1 - \hat{L}_1}\right) + \hat{L}_1\hat{x} - \hat{L}_1\right] \tag{75}$$

If $(E_q - \Psi_i)$ is small, the curvature of the acquiring curve is approximately its second derivative and this curvature is proportional to the bank angle. The value of L_1 should be such that the maximum and minimum bank angles are numerically equal in order to minimize the maximum bank angle needed during the acquiring segment of the flightpath. This result can be achieved by setting

$$\left|\left(\frac{d^2\hat{y}}{d\hat{x}^2}\right)_1\right|_{\hat{x}=\frac{\hat{L}_1}{2}} = \left|\left(\frac{d^2\hat{y}}{d\hat{x}^2}\right)_2\right|_{\hat{x}=(\frac{1-\hat{L}_1}{2})} \tag{76}$$

Substituting for the second derivatives from equations (70) and (73) into equation (76) gives

$$\frac{(1 + \hat{L}_1)\pi}{\hat{L}_1} = \frac{\hat{L}_1\pi}{1 - \hat{L}_1} \tag{77}$$

The solution of equation (77) is

$$\hat{L}_1 = \frac{1}{\sqrt{2}} = 0.70711 \tag{78}$$

With the value of $\hat{L}_1$ given by equation (78), the maximum bank angle during the acquiring maneuver is given by

$$\phi_{max} = \arctan\left(\frac{0.002055(E_q - \Psi_i)v_t^2}{L}\right) \tag{79}$$

where E_q and Ψ_i are in degrees. For example, if $v_t = 200$ ft/sec, $(E_q - \Psi_i) = 10$ deg, and $L = 4,000$ ft, then equation (79) gives $\phi_{max} = 11.6$ deg.

20

CONCLUDING REMARKS

Several problems with the HUD drive laws given in references 1 and 2 have been identified and solutions have been proposed. All these solutions have been flight tested successfully in the VSRA Phase IIA flight test program. Of all the problems addressed, the one whose solution appears to be marginal is that of acquiring the first segment of the synthesized flightpath when the aircraft's course differs significantly from the heading of the first straight segment (identified as problem (7) in the Introduction). The synthesized-acquiring-curve approach given herein can be regarded only as an interim solution satisfactory for relatively small course errors (less than 15 deg). One pilot considered the "S" turn maneuver associated with the acquiring curve, coupled with the sensitivity of the ghost aircraft to lateral flightpath errors, to be impractical as an instrument procedure. A much better approach, although one requiring a more complicated algorithm, is to implement a two-circle flightpath synthesis requiring the pilot to correct his course to that of the first straight segment by making a simple turn in one direction only.

REFERENCES

1. Merrick, Vernon K., Farris, Glenn G.; and Vanags, Andrejs A.: A Head Up Display for Application to V/STOL Aircraft Approach and Landing. NASA TM-102216, January 1990.

2. Merrick, Vernon K.; Moralez, Ernesto; Stortz, Michael W., Hardy, Gordon H.; and Gerdes, Ronald M.. Simulation Evaluation of a Speed-Guidance Law for Harrier Transitions. NASA TM-102853, April 1991.

3. Schroeder, J. A., and Merrick, V. K.: Control and Display Combinations for Blind Landings. AIAA J. Guidance, Control, and Dynamics, vol. 15, no. 3, May-June 1992.

4. Dorr, D. W.; Moralez, E., III; and Merrick, V. K.: Simulation and Flight Test Evaluation of Head-Up-Display Guidance for Harrier Transitions. AIAA Aircraft Design Systems Meeting, AIAA Paper 92-4233, August 1992.

APPENDIX A

FLIGHTPATH SYNTHESIS

Preliminaries

It is assumed that the onboard navigation sensors provide sufficient information and that there is sufficient processing capability to permit onboard continuous synthesis of a reference flightpath that is a member of a predefined class of flightpaths. When the synthesized flightpath is acceptable to the pilot he/she selects it by "freezing" the synthesizing process.

The class of approach flightpaths used in conjunction with the HUD is illustrated in figure A-1. A set of constant parameters, identified in the following section, must be provided to the synthesizing system so that it can construct an appropriate flightpath within the predefined class of flightpaths. This flightpath is constructed as follows: from any aircraft position, the nominal, instantaneous, reference flightpath is defined as the line tangential to one of the circles shown in figure A-1 and passing through the aircraft, followed by a segment of the circle and finally by a predefined straight-line segment. The flightpath ends either at touchdown or at the station-keeping point. The horizontal plane is divided into two parts by a line coincident with the final straight segment. This division determines which of the two circles will be used. If the aircraft is flown across the boundary during the process of continuous flightpath synthesis, the first segment of the flightpath moves from being tangential to one circle to
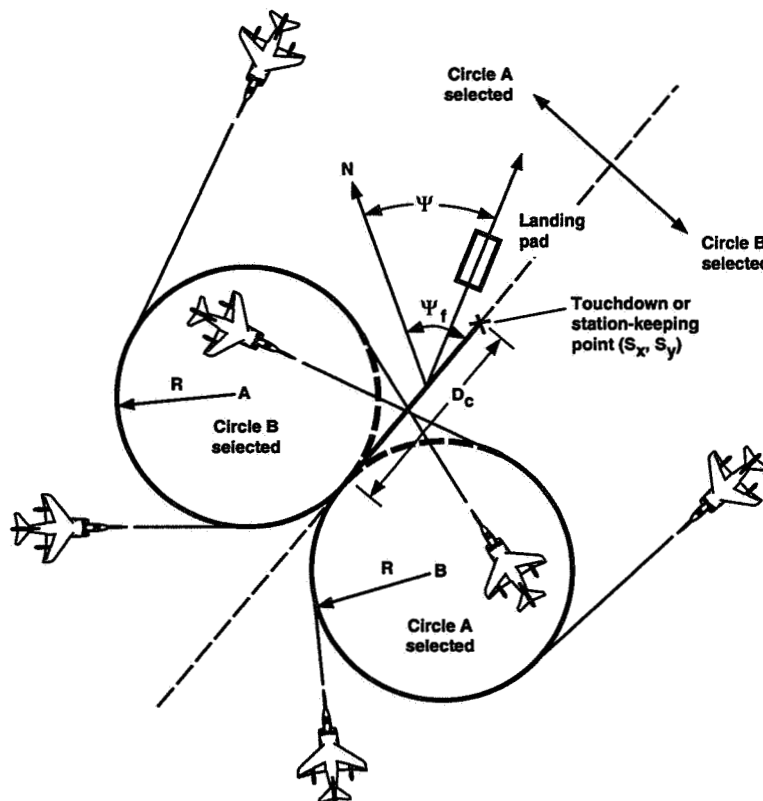

Figure A-1. Class of reference flightpaths.

being tangential to the other. If the aircraft passes within either of the circles before the pilot selects a flightpath, the first segment switches from the circle entered to the other circle (fig. A-1).

Required Data

The following information must be provided to the system:

S_x, S_y	touchdown, or station-keeping point coordinates in the landing-pad reference frame
Ψ	landing-pad heading ($0 \leq \Psi < 360$ deg)
Ψ_f	heading of the final flightpath segment ($0 \leq \Psi_f < 360$ deg)
D_c	nominal length of the final flightpath segment (fig. A-1)
$R_{l(min)}$	nominal minimum radius of the horizontal flightpath circles
$\hat{T}_p$	normalized nominal maximum length of the portion of the ordinate of the blending curve replacing a portion of a straight segment
$\bar{N}_{0(min)}$	minimum permitted value of $\bar{\nu}_0$
ΔD_{ac}	minimum desirable distance along the curved segment of the flightpath

These parameters are generally constant and they have suitable default values, but they may be changed by the pilot any time prior to the time the reference flightpath is selected. After the reference flightpath has been selected, no further changes in these parameters can be made. In addition to these parameters, the navigation system must continuously provide the coordinates (x_a, y_a) of the aircraft in the landing-pad reference frame.

Synthesis

Calculations before flightpath select– Figure A-2 shows the geometry of the flightpath. The coordinates of point C and the centers of the circles can be calculated from the basic data. The coordinates of point C are given by the equations

$$C_x = S_x - D_c \cos \Delta\Psi_f \tag{A-1}$$

$$C_y = S_y - D_c \sin \Delta\Psi_f \tag{A-2}$$

where $\Delta\Psi_f$ is the heading of the final flightpath segment relative to the x-axis of the landing pad. It is given by the equation

$$\Delta\Psi_f = \Psi_f - \Psi \qquad 0 \leq \Delta\Psi_f < 360 \text{ deg} \tag{A-3}$$

The coordinates $(R^{(i)}_{l(min)x}, R^{(i)}_{l(min)y})$ of the centers of the minimum-radius circles are given by the equations

$$R^{(i)}_{l(min)x} = C_x - iR_{l(min)} \sin \Delta\Psi_f \tag{A-4}$$

$$R^{(i)}_{l(min)y} = C_y + iR_{l(min)} \cos \Delta\Psi_f \tag{A-5}$$
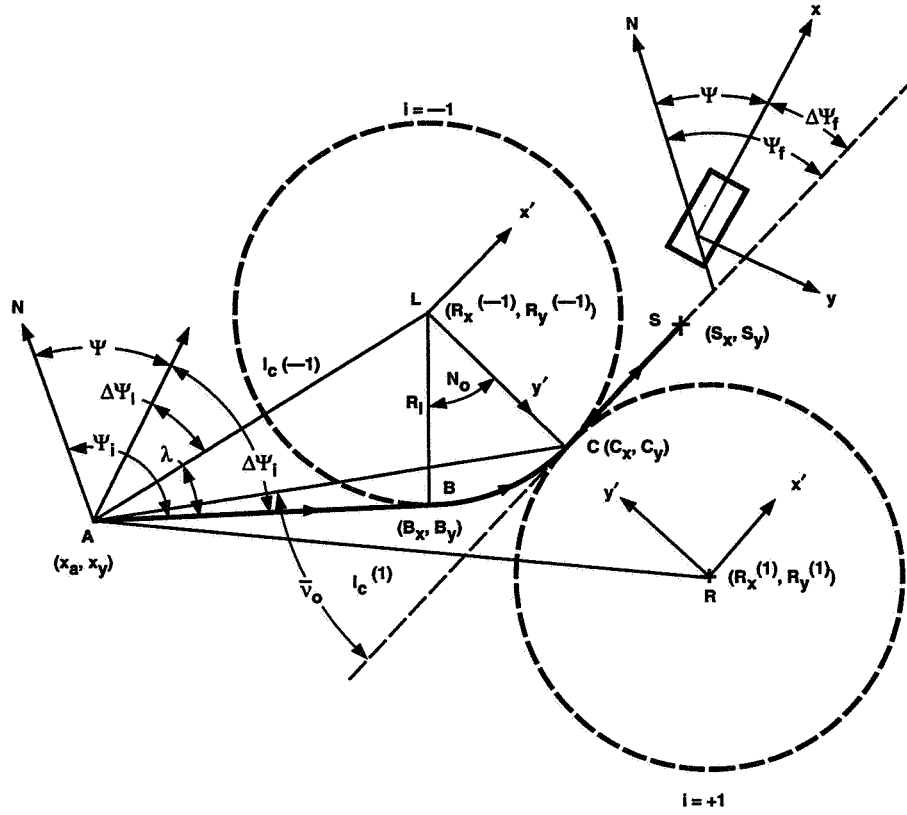
24

Figure A-2. Flightpath geometry.

where $(i = +1)$ or $(i = -1)$ denotes the circle for flight in the clockwise or counterclockwise directions, respectively.

The appropriate circle depends on the distances $l_c^{(i)}$, $i = +1$, or $i = -1$, of the aircraft from the centers of the circles, given by

$$l_c^{(i)} = \sqrt{(x_a - R_{l(min)x}^{(i)})^2 + (y_a - R_{l(min)y}^{(i)})^2} \quad \text{where } i = +1, -1 \tag{A-6}$$

with the circle-selection conditions

$$\text{if } l_c^{(+1)} < R_{l(min)}, \text{ then } i = -1$$

$$\text{if } l_c^{(-1)} < R_{l(min)}, \text{ then } i = +1$$

$$\text{if } l_c^{(+1)} \geq R_{l(min)} \text{ and } l_c^{(-1)} \geq R_{l(min)} \text{ and } l_c^{(+1)} > l_c^{(-1)}, \text{ then } i = -1$$

$$\text{if } l_c^{(+1)} \geq R_{l(min)} \text{ and } l_c^{(-1)} \geq R_{l(min)} \text{ and } l_c^{(+1)} \leq l_c^{(-1)}, \text{ then } i = +1$$

During the testing of the flightpath synthesis given in reference 1, the pilot was directed to make the heading change too abruptly when the heading change due to the turn from the initial to the final straight flightpath segments was less than about ±15 deg; the result was that large bank angles were

required for only short periods of time. This type of maneuver is an abnormal piloting technique even for a visual approach. The method used herein to overcome this problem is to allow the flightpath-circle radius to increase when the required heading change is less than about ±15 deg. This radius increase may be specified in many ways; the one adopted herein was chosen for its computational simplicity. It requires the calculation of the length l_{ac} of the line AC and the angle $\bar{\nu}_0$ between the line AC and the final straight segment (fig. A-2). The value of l_{ac} is given by

$$l_{ac} = \sqrt{(x_a - C_x)^2 + (y_a - C_y)^2}$$ (A-7)

The angle $\bar{\nu}_0$ is determined by first calculating the heading of the line AC, given by the equation

$$\psi_{ac} = \arctan\left(\frac{C_y - y_a}{C_x - x_a}\right) + \Psi \qquad 0 \le \psi_{ac} < 360 \text{ deg}$$ (A-8)

and then subtracting the heading of the final straight segment, taking into account the particular flightpath circle (value of i) being used. The calculation may be performed by using the equation

$$\bar{\nu}_0 = 180(i + 1) - i(\psi_{ac} - \Psi_f) \qquad 0 \le \bar{\nu}_0 < 360 \text{ deg}$$ (A-9)

The value of $\bar{\nu}_0$ must be limited in order to avoid excessive circle radii. This limited $\bar{\nu}_0$, designated $\bar{\nu}_{0l}$, is given by

$$\bar{\nu}_{0l} = \begin{cases} \bar{\nu}_0 & \text{if } \bar{\nu}_0 \ge \bar{N}_{0(min)} \\ \bar{N}_{0(min)} & \text{if } \bar{\nu}_0 < \bar{N}_{0(min)} \end{cases}$$ (A-10)

The radius of the flightpath circle is increased from the minimum, $R_{l(min)}$, when the headings of the initial and final flightpath segments differ by less than about ±15 deg to a maximum, $R_{l(max)}$, whose value is controlled by specifying the minimum acceptable distance, ΔD_{ac}, to be flown along the curved flightpath segment. The instantaneous circle radius, r_l, and the blend parameter, $\hat{v}$, are defined by the following relationships, which are shown graphically in figure A-3.

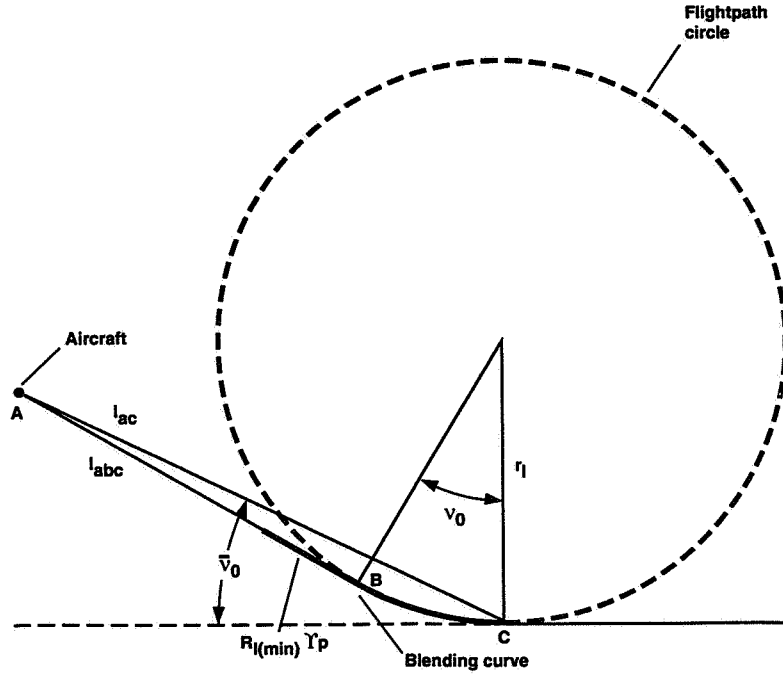If $\bar{\nu}_{0l} \le 180\Delta D_{ac}/\pi R_{l(min)}$, then

$$r_l = \frac{180\Delta D_{ac}}{\pi \bar{\nu}_{0l}}$$ (A-11)

The value of r_l obtained from equation (A-11) must be bounded above to avoid, for as long as possible, flying into the interior of the circle prior to flightpath select—an event that would cause the synthesis procedure to switch to the other circle—and bounded below by the minimum radius. Specifically,

$$r_{ll} = \begin{cases} 180(l_{ac} - R_{l(min)}\hat{\Upsilon}_p)/\pi\bar{\nu}_{0l} & \text{if } r_l > 180(l_{ac} - R_{l(min)}\hat{\Upsilon}_p)/\pi\bar{\nu}_{0l} \\ R_{l(min)} & \text{if } r_l < R_{l(min)} \end{cases}$$ (A-12)

and the corresponding value of $\hat{v}$ is given by

$$\hat{v} = \hat{\Upsilon}_p R_{l(min)}/r_{ll}$$ (A-13)

26

Figure A-3. Geometrical condition restricting the flightpath radius.

From inspection of the figure, the condition for the aircraft to be either outside or at the start of the blending curve is

$$l_{abc} \geq 180 r_l \nu_0 / \pi + R_{l(min)} \Upsilon_p$$

but for small values of ν_0, $l_{abc} \approx l_{ac}$ and $\bar{\nu}_0 \approx \nu_0$. Therefore,

$$r_l \leq 180(l_{ac} - R_{l(min)} \Upsilon_p)/\pi \bar{\nu}_0$$

On the other hand, if $\bar{\nu}_{0l} > 180 \Delta D_{ac} / \pi R_{l(min)}$, then

$$r_{ll} = R_{l(min)} \tag{A-14}$$

$$\hat{v} = \Upsilon_p \tag{A-15}$$

It follows from equations (A-10) and (A-11) that the maximum possible flightpath circle radius, $R_{l(max)}$, is given by

$$R_{l(max)} = \frac{180 \Delta D_{ac}}{\pi \bar{N}_{0(min)}} \tag{A-16}$$

Having determined the appropriate circle (value of i) along with its radius, r_{ll}, and the blend parameter, $\hat{v}$, the coordinates (r_{llx}, r_{lly}) of this circle in the landing-pad reference frame are calculated

27

by using the equations

$$r_{llx} = C_x - ir_{ll} \sin \Delta \Psi_f \qquad \text{(A-17)}$$

$$r_{lly} = C_y + ir_{ll} \cos \Delta \Psi_f \qquad \text{(A-18)}$$

Further calculations require knowledge of the angles $\delta\psi_l$ and λ (fig. A-2). Angle $\delta\psi_l$ is the angle between the line from the aircraft to the center of the appropriate circle (AL or AR of fig. A-2) and the x-axis of the landing pad. Angle λ is the angle between AL or AR and the first flightpath segment. These two quantities are calculated from the equations

$$\delta\psi_l = \frac{180}{\pi} \arctan\left(\frac{r_{lly} - y_a}{r_{llx} - x_a}\right) \qquad 0 \le \delta\psi_l < 360 \text{ deg} \qquad \text{(A-19)}$$

$$\lambda = \frac{180}{\pi} \arcsin\left(\frac{r_{ll}}{l_c}\right) \qquad \text{(A-20)}$$

where l_c is the distance from the aircraft to the center of the circle that has been identified by the previous calculations; it is given by the equation

$$l_c = \sqrt{(x_a - r_{llx})^2 + (y_a - r_{lly})^2} \qquad \text{(A-21)}$$

The track angle of the initial flightpath segment relative to the x-axis of the landing pad, $\delta\psi_i$, may now be calculated from the equation

$$\delta\psi_i = \delta\psi_l - i\lambda \qquad 0 \le \delta\psi_i < 360 \text{ deg} \qquad \text{(A-22)}$$

and the initial flightpath heading is given by

$$\psi_i = \Psi + \delta\psi_i \qquad 0 \le \psi_i < 360 \text{ deg} \qquad \text{(A-23)}$$

The coordinates b_x, b_y of point B at the start of the circular segment may now be calculated using the equations

$$b_x = r_{llx} + ir_{ll} \sin \delta\psi_i \qquad \text{(A-24)}$$

$$b_y = r_{lly} - ir_{ll} \cos \delta\psi_i \qquad \text{(A-25)}$$

The angle ν_0 that the circular segment subtends at the center of the circle is obtained using the equation

$$\nu_0 = 180(i + 1) - i(\psi_i - \Psi_f) \qquad 0 \le \nu_0 < 360 \text{ deg} \qquad \text{(A-26)}$$

The quantities $i, \delta\psi_i, \psi_i, b_x, b_y, r_{ll}, r_{llx}, r_{lly}$, and ν_o are calculated continuously up to the instant that the pilot selects the reference flightpath. After flightpath selection, these quantities remain constant

28

at their values at the instant of flightpath selection and they are subsequently designated by the uppercase symbols I, $\Delta\Psi_i$, Ψ_i, B_x, B_y, R_{ll}, R_{llx}, R_{lly}, and N_0.

Calculations after flightpath select– The blending-curve constants are calculated immediately after flightpath selection. It should be recognized that there is a maximum possible value for $\hat{v}$ that may be less than the value of $\hat{\Upsilon}_p$ requested. This maximum is defined by two possibilities: first, the appropriate solution resulting in a proper fit of the cubic blending curve to both the straight and circular segments holds only if

$$\hat{v} \le \sqrt{\frac{2}{27}} \tag{A-27}$$

and second, the value of $\hat{v}$ cannot be greater than that which causes the blending curves for entry and exit to meet in the middle of the circular segment. The condition expressing this limitation is

$$\hat{v} \le \sin\frac{N_0}{2} - 2\left(\sin\frac{N_0}{2}\right)^3 \qquad N_0 < 2\arcsin\sqrt{\left(\frac{1}{6}\right)} \tag{A-28}$$

The final value of $\hat{v}$ is then given by the lesser of the limiting values given by equations (A-13) or (A-15), (A-27) and (A-28). This value is designated $\hat{\Upsilon}$

The blending-curve constants are obtained by first defining a quantity $\hat{F}$ as follows:

$$\hat{F} \stackrel{\text{def}}{=} \arccos\left(-\hat{\Upsilon}\sqrt{\frac{27}{2}}\right) \tag{A-29}$$

The normalized distance $\widehat{\widehat{X}}$ measured along the straight segment over which the blending curve replaces the circular arc segment is then given by

$$\widehat{\widehat{X}} = \sqrt{\frac{2}{3}}\cos\left(\frac{\hat{F} + 4\pi}{3}\right) \tag{A-30}$$

and the normalized distance $\widehat{X}$ measured along the straight segment is then given by

$$\widehat{X} = \widehat{\widehat{X}} + \hat{\Upsilon} \tag{A-31}$$

The defining constant of the cubic blending curve, $\widehat{\Xi}$, is then calculated from the equation

$$\widehat{\Xi} = \frac{\widehat{\widehat{X}}}{3\widehat{X}^2\sqrt{1 - \widehat{\widehat{X}}^2}} \tag{A-32}$$

If $\hat{\Upsilon} = 0$, then $\widehat{\widehat{X}}$ and $\widehat{X}$ are both zero and $\widehat{\Xi}$ from equation (A-32) is indeterminate. In order to recover the flightpath-synthesis equations of reference 1, which are appropriate to the case where $\hat{\Upsilon} = 0$, it is necessary to define $\widehat{\Xi}$ to be zero.

The true radius $\bar{R}_{ll}$ of the flightpath circle is obtained from the nominal radius R_{ll} by using the equation

$$\bar{R}_{ll} = \frac{R_{ll}}{\widehat{\Xi}\widehat{X}^3 + \sqrt{1 - \widehat{X}^2}}$$

(A-33)

If the quantity E is defined as follows,

$$E \overset{\text{def}}{=} \arcsin \widehat{X}$$

(A-34)

then the true flightpath circular segment subtends an angle $\bar{N}_0$ given by

$$\bar{N}_0 = N_0 - 2E$$

(A-35)

Relationships (A-29)–(A-35) complete the calculation of the blending-curve constants; we now will calculate the key ranges (measured along the true reference flightpath) at the points C_1, C_2, B_1, B_2, and A. First, it is necessary to calculate the lengths of the two principal segments of the blending curve corresponding to the normalized ordinates $\widehat{\Upsilon}$ and $\widehat{X}$. These lengths can be obtained from the equation

$$\hat{s}(\hat{x}) = \hat{x} + 0.9\widehat{\Xi}^2\hat{x}^5 - 1.125\widehat{\Xi}^4\hat{x}^9$$

(A-36)

where

$\hat{x}$ normalized blending-curve abscissa
$\hat{s}(\hat{x})$ normalized length of the blending curve

The key ranges $D_{c_1}, D_{c_2}, D_{b_1}$, and D_{b_2} are then given by

$$D_{c_1} = D_c - \bar{R}_{ll}\widehat{\Upsilon}$$

(A-37)

$$D_{c_2} = D_{c_1} + \bar{R}_{ll}\hat{s}(\widehat{X})$$

(A-38)

$$D_{b_2} = D_{c_2} + \frac{\pi\bar{R}_{ll}\bar{N}_0}{180}$$

(A-39)

$$D_{b_1} = D_{b_2} + D_{c_2} - D_{c_1}$$

(A-40)

The instantaneous range D_a of the aircraft at flightpath selection is given by

$$D_a = l_c \cos \Lambda - \bar{R}_{ll}\widehat{\Upsilon} + D_{b_1}$$

(A-41)

The quantities $\bar{R}_{ll}, \widehat{\Xi}, \bar{N}_0, \widehat{\Upsilon}, D_{c_1}, D_{c_2}, D_{b_1}, D_{b_2}$, and D_a are calculated once only for subsequent use in the guidance equations (appendix B).

ɟ

APPENDIX B

GUIDANCE

Lateral Guidance

Lateral guidance is provided by the ghost-aircraft symbol, and the lateral-guidance law is provided by the geometric relationship between the flightpath symbol and the ghost (fig. 16 of ref. 1). Calculation of the azimuth angle of the ghost, μ_g, requires knowledge of the range, d, the lateral offset of the aircraft from the reference-flightpath track, δy, and the heading of the reference flightpath, ψ_t. In addition, the ghost roll angle, ϕ_g, given by

$$\phi_g = \frac{180}{\pi} \arctan\left(\frac{v_t^2}{\rho g}\right) \tag{B-1}$$

requires knowledge of the reference-flightpath curvature, $1/\rho$, at the aircraft's position (identified by its range, d).

The quantities $I, \Delta\Psi_i, \Psi_i, B_x, B_y, \bar{R}_{ll}, R_{llx}, R_{lly}, \bar{N}_0, \hat{\Upsilon}, D_{c_1}, D_{c_2}, D_{b_1}, D_{b_2}$, and D_a have been calculated by the flightpath-synthesis algorithm (appendix A). The reference flightpath is now modified slightly by the addition of the acquiring segment; this segment is defined by the following five quantities:

L overall length of the acquiring curve segment

K_{ab} ratio of the lengths of the acquiring curve and the initial straight segment

$\hat{L}_1$ normalized length from the start of the acquiring curve to the point of roll reversal

E_q heading of the HUD flightpath symbol at the instant of flightpath select

Ψ_i heading of the initial flightpath segment

The quantity $\hat{L}_1$ is normally set equal to $1/\sqrt{2}$, but it may be changed by the pilot. The length L is normally set equal to the distance of the aircraft from the start of the turn entry, $D_a - D_{b_1}$, but it may be changed to a fraction of this distance, K_{ab}, by the pilot. Specifically,

$$L = K_{ab}(D_a - D_{b_1}) \tag{B-2}$$

The heading E_q ($0 \leq E_q < 360$ deg) is set equal to $\epsilon_q + \Psi_a$ (ϵ_q is given by eq. (15) of ref. 1) at the instant of flightpath select and is constant thereafter. The equations needed to determine the quantities d, δy, and ψ_t depend on which segment of the reference flightpath corresponds with the aircraft's location (fig. B-1).

For segments AA_1, A_1B_1, B_1B_2, and B_2C_2, the normalized coordinates of the aircraft ($\hat{x}_{2a}, \hat{y}_{2a}$) in an axis system with origin at B and x-axis along the line AB are required and are given by

$$\hat{x}_{2a} = [(x_a - B_x)\cos\Delta\Psi_i + (y_a - B_y)\sin\Delta\Psi_i]/\bar{R}_{ll} + \hat{\Upsilon} \tag{B-3}$$

$$\hat{y}_{2a} = -I[(x_a - B_x)\sin\Delta\Psi_i - (y_a - B_y)\cos\Delta\Psi_i]/\bar{R}_{ll} \tag{B-4}$$
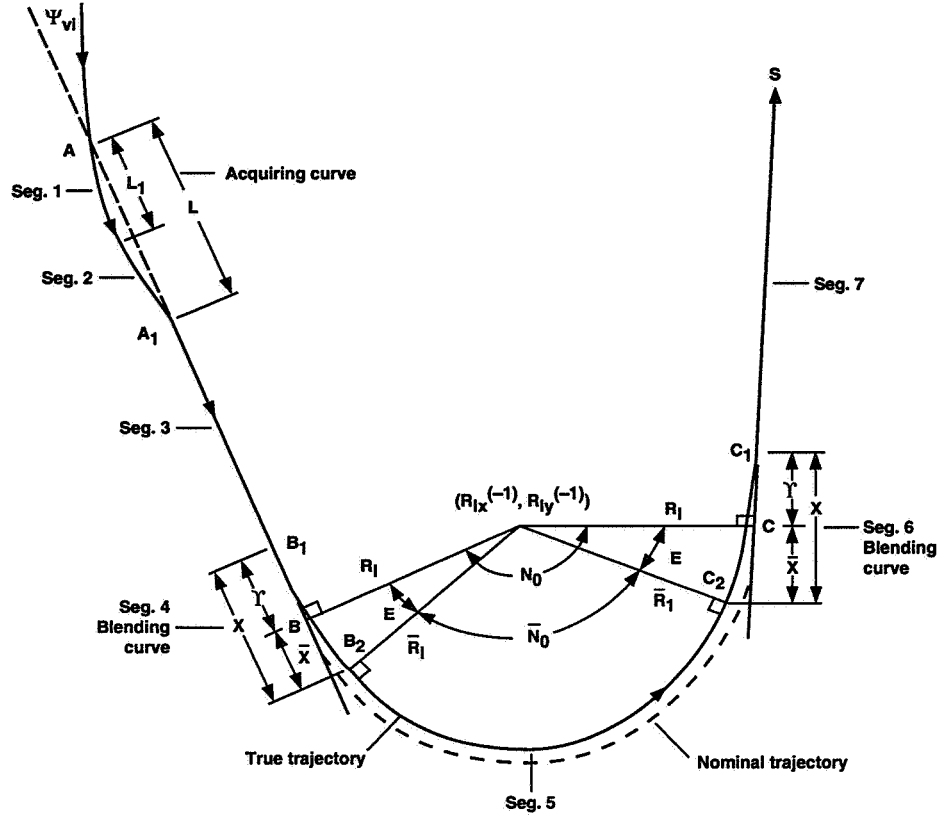
31

Figure B-1 Flightpath segments.

Also required for calculations in segments AA_1 and A_1B is the range, D_{a_1}, of the point A_1 at the end of the acquiring curve, given by

$$D_{a_1} = D_a - L \tag{B-5}$$

The parameters within the acquiring segment AA_1 defined by $D_a \geq d > D_{a_1}$

where

$$d = D_{b_1} - \bar{R}_{ll}\hat{x}_{2a} \tag{B-6}$$

$$\hat{x} = (D_a - d)/L \tag{B-7}$$

are given by

$$\delta y = I\bar{R}_{ll}\hat{y}_{2a} - \frac{\pi L\Psi_{vi}}{360}\left[\frac{\hat{L}_1(1 + \hat{L}_1)}{\pi}\sin \pi\left(\frac{\hat{x}}{\hat{L}_1}\right) + (1 - \hat{L}_1)\hat{x}\right] \tag{B-8}$$

$$\psi_t = \Psi_i + \frac{\pi\Psi_{vi}}{360}\left[(1 + \hat{L}_1)\cos \pi\left(\frac{\hat{x}}{\hat{L}_1}\right) + (1 - \hat{L}_1)\right] \tag{B-9}$$

$$\frac{1}{\rho} = -\frac{\pi^2(1 + \hat{L}_1)\Psi_{vi}}{360L\hat{L}_1}\sin \pi\left(\frac{\hat{x}}{\hat{L}_1}\right) \tag{B-10}$$

if $0 \leq \hat{x} \leq \hat{L}_1$

32

and by

$$\delta y = I \bar{R}_{ll} \hat{y}_{2a} - \frac{\pi L \Psi_{vi}}{360} \left[\frac{\widehat{L}_1 (1 - \widehat{L}_1)}{\pi} \sin \pi \left(\frac{\hat{x} - \widehat{L}_1}{1 - \widehat{L}_1} \right) + \widehat{L}_1 \hat{x} - \widehat{L}_1 \right] \tag{B-11}$$

$$\psi_t = \Psi_i - \frac{\pi \Psi_{vi}}{360} \left[\widehat{L}_1 \cos \pi \left(\frac{\hat{x} - \widehat{L}_1}{1 - \widehat{L}_1} \right) + \widehat{L}_1 \right] \tag{B-12}$$

$$\frac{1}{\rho} = \frac{\pi^2 \widehat{L}_1 \Psi_{vi}}{360 L (1 - \widehat{L}_1)} \sin \pi \left(\frac{\hat{x} - \widehat{L}_1}{1 - \widehat{L}_1} \right) \tag{B-13}$$

where

$$\Psi_{vi} = E_q - \Psi_i \qquad (0 \le \Psi_{vi} < 360 \text{ deg}) \tag{B-14}$$

if $\widehat{L}_1 < \hat{x} \le 1$.

It should be noted here that if an acquiring curve is not required ($K_{ab} = 0$), then the calculations of equations (B-5)–(B-14) must be omitted.

The parameters within the initial straight segment $A_1 B_1$ defined by $D_{a_1} \ge d > D_{b_1}$

where

$$d = D_{b_1} - \bar{R}_{ll} \hat{x}_{2a} \tag{B-15}$$

are

$$\delta y = I \bar{R}_{ll} \hat{y}_{2a} \tag{B-16}$$

$$\psi_t = \Psi_i \tag{B-17}$$

$$\frac{1}{\rho} = 0 \tag{B-18}$$

The parameters within the turn-entry blend segment $B_1 B_2$ defined by $D_{b_1} \ge d > D_{b_2}$

where

$$d = D_{b_1} - \bar{R}_{ll} \hat{s}(\hat{x}_p) \tag{B-19}$$

are

$$\delta y = [\text{sign} \, (\hat{y}_{2a} - \widehat{\Xi} \hat{x}_{2a}^3)] I \bar{R}_{ll} \sqrt{(\hat{x}_{2a} - \hat{x}_p)^2 + (\hat{y}_{2a} - \hat{y}_p)^2} \tag{B-20}$$

$$\psi_t = \Psi_i - \frac{I 180}{\pi} \arctan \, (3 \widehat{\Xi} \hat{x}_p^2) \tag{B-21}$$

$$\frac{1}{\rho} = \frac{I 6 \widehat{\Xi} \hat{x}_p}{\bar{R}_{ll} (1 + 9 \widehat{\Xi}^2 \hat{x}_p^4)^{3/2}} \tag{B-22}$$

For the segment B_2C_2, the coordinates of the aircraft (x_{1a}, y_{1a}) are required in an axis system whose origin is at the center of the appropriate circle and whose x-axis is parallel to the final flightpath segment (fig. A-2). These coordinates are given by

$$x_{1a} = (x_a - R_{llx}) \cos \Delta \Psi_f + (y_a - R_{lly}) \sin \Delta \Psi_f \tag{B-23}$$

$$y_{1a} = I[(x_a - R_{llx}) \sin \Delta \Psi_f - (y_a - R_{lly}) \cos \Delta \Psi_f] \tag{B-24}$$

In addition, the angle ν subtended at the center of the circle by the remaining part of the circular-arc segment is required and is given by

$$\nu = \frac{180}{\pi} \arctan\left(\frac{-x_{1a}}{y_{1a}}\right) \qquad 0 \le \nu < 360 \text{ deg} \tag{B-25}$$

The parameters within the circular segment B_2C_2 defined by $D_{b_2} \ge d > D_{c_2}$

where

$$d = D_{c_2} + \frac{\pi}{180} \bar{R}_{ll} (\nu - E) \tag{B-26}$$

are

$$l_a = \sqrt{(x_a - R_{llx})^2 - (y_a - R_{lly})^2} \tag{B-27}$$

$$\delta y = I(\bar{R}_{ll} - l_a) \tag{B-28}$$

$$\psi_t = \Psi_f - I\nu \tag{B-29}$$

$$\frac{1}{\rho} = \frac{I}{\bar{R}_{ll}} \tag{B-30}$$

For segments C_2C_1 and C_1S, the normalized coordinates of the aircraft $(\hat{x}_{2a}, \hat{y}_{2a})$ are redefined relative to an axis system with origin at C_1 and x-axis along the line SC; they are now given by

$$\hat{x}_{2a} = -[(x_a - S_x) \cos \Delta \Psi_f + (y_a - S_y) \sin \Delta \Psi_f + D_{c_1}]/\bar{R}_{ll} \tag{B-31}$$

$$\hat{y}_{2a} = -I[-(y_a - S_y) \cos \Delta \Psi_f + (x_a - S_x) \sin \Delta \Psi_f]/\bar{R}_{ll} \tag{B-32}$$

The parameters within the turn-exit blend segment C_2C_1 defined by $D_{c_2} \ge d > D_{c_1}$

where

$$d = D_{c_1} + \bar{R}_{ll} \hat{s}(\hat{x}_p) \tag{B-33}$$

are

$$\delta y = [\text{sign}(\hat{y}_{2a} - \widehat{\Xi} \hat{x}_{2a}^3)] I \bar{R}_{ll} \sqrt{(\hat{x}_{2a} - \hat{x}_p)^2 + (\hat{y}_{2a} - \hat{y}_p)^2} \tag{B-34}$$

$$\psi_t = \Psi_f - \frac{I180}{\pi} \arctan\left(3\widehat{\Xi} \hat{x}_p^2\right) \tag{B-35}$$

$$\frac{1}{\rho} = \frac{I6\widehat{\Xi}\hat{x}_p}{\bar{R}_{ll}(1 + 9\widehat{\Xi}^2 \hat{x}_p^4)^{3/2}} \tag{B-36}$$

34

The parameters within the final straight segment $C_1 S$ defined by $D_{c_1} \geq d$

where

$$d = D_{c_1} + \bar{R}_{ll} \hat{x}_{2a} \tag{B-37}$$

are

$$\delta y = I \bar{R}_{ll} \hat{y}_{2a} \tag{B-38}$$

$$\psi_t = \Psi_f \tag{B-39}$$

$$\frac{1}{\rho} = 0 \tag{B-40}$$

The quantities $\hat{x}_p$ and $\hat{y}_p$ are the normalized coordinates of the foot of the perpendicular from the aircraft to the blending curve; they are given by

$$\hat{x}_p = \hat{x}_{2a}\left[1 + \frac{3\widehat{\Xi}\hat{x}_{2a}(\hat{y}_{2a} - \widehat{\Xi}\hat{x}_{2a}^3)}{1 - 3\widehat{\Xi}\hat{x}_{2a}(2\hat{y}_{2a} - 5\widehat{\Xi}\hat{x}_{2a}^3)}\right] \tag{B-41}$$

$$\hat{y}_p = \widehat{\Xi}\hat{x}_p^3 \tag{B-42}$$

The quantity $\hat{s}(\hat{x}_p)$ is the normalized distance of the point $(\hat{x}_p, \hat{y}_p)$, measured along the blending curve from the point where the transition curve and a straight segment meet; it is given by

$$\hat{s}(\hat{x}_p) = \hat{x}_p + 0.9\widehat{\Xi}^2\hat{x}_p^5 - 1.125\widehat{\Xi}^4\hat{x}_p^9 \tag{B-43}$$

Vertical Guidance

Vertical guidance, like lateral guidance, is provided by the ghost-aircraft symbol. At the instant of guidance select, the vertical flightpath is defined as shown in figure B-2. This flightpath consists of a constant-altitude segment, AJ_1, at the altitude of flightpath select, an approach segment, $J_2 S$, with a constant flightpath angle, Γ, and a circular connecting segment, $J_1 J_2$. The following information must be provided to the system in order to define this flightpath:

H_{ri} aircraft altitude at guidance select
H hover altitude
R_v radius of the vertical flightpath circle, $J_1 J_2$
Γ approach flightpath angle

The quantities H, R_v, and Γ are set by the pilot, with default values of 50 ft, 30,000 ft, and –3 deg, respectively.
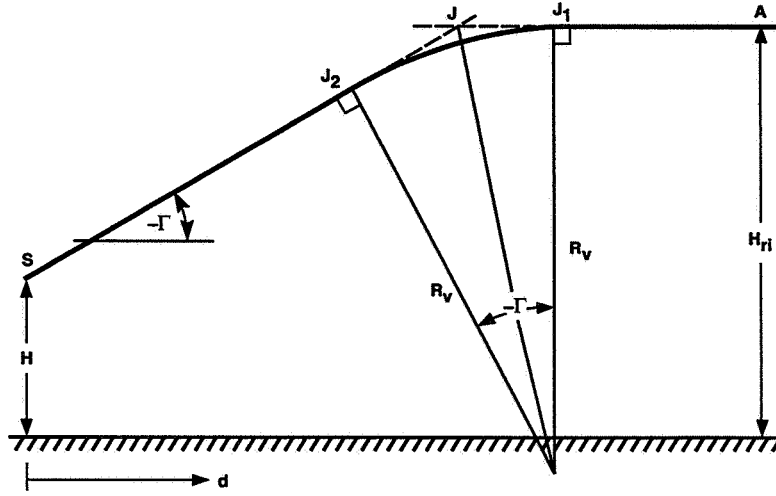
Figure B-2. Vertical flightpath geometry.

From figure B-2, the ranges at points J, J_1, and J_2 are given by

$$D_j = (H - H_{ri})/\tan(\Gamma) \tag{B-44}$$

$$D_{j_1} = D_j - R_v \tan\left(\frac{\Gamma}{2}\right) \tag{B-45}$$

$$D_{j_2} = D_{j_1} + R_v \tan(\Gamma) \tag{B-46}$$

The elevation angle of the ghost relative to the aircraft, η_g, is expressed in reference 1 (eq. (19)) as

$$\eta_g = \frac{180}{\pi} \arctan\left(\frac{h_g - h}{\delta x_{gh}}\right) \tag{B-47}$$

where

h_g	altitude of the ghost aircraft
h	altitude of the aircraft
δx_{gh}	lead distance of the ghost for vertical tracking

The ghost altitude is given by

$$h_g = h_r + \delta x_{gh} k_{wg} \tan \gamma_t \tag{B-48}$$

where

h_r	aircraft reference altitude
γ_t	reference flightpath angle at the aircraft's range
k_{wg}	ghost lead blending gain

The ghost lead blending gain k_{wg} is defined in reference 1 (eq. (22)).

36

From equations (B-47) and (B-48), η_g may be expressed as

$$\eta_g = \arctan\left(k_{wg}\tan\gamma_t - \frac{\delta h}{\delta x_{gh}}\right) \tag{B-49}$$

where $\delta h = h - h_r$ is the altitude error of the aircraft relative to the reference flightpath.

Determination of η_g, therefore, requires knowledge of the altitude error, δh, and the reference flightpath angle, γ_t. These quantities depend on which segment of the reference flightpath corresponds with the aircraft's location.

The parameters within the constant-altitude segment AJ_1 defined by $D_a \geq d > D_{j_1}$

are

$$\gamma_t = 0 \tag{B-50}$$

$$\delta h = h - H_{ri} \tag{B-51}$$

The parameters within the circular segment $J_1 J_2$ defined by $D_{j_1} \geq d > D_{j_2}$

are

$$\gamma_t = \arcsin[(d - D_{j_1})/R_v] \tag{B-52}$$

$$\delta h = h - H_{ri} + R_v(1 - \cos\gamma_t) \tag{B-53}$$

The parameters within the constant-flightpath-angle segment $J_2 S$ defined by $D_{j_2} \geq d \geq 0$

are

$$\gamma_t = \Gamma \tag{B-54}$$

$$\delta h = h - H + d\tan(\Gamma) \tag{B-55}$$

REPORT DOCUMENTATION PAGE

Public reporting burden for this collection of information is estimated to average 1 hour per response, including the time for reviewing instructions, searching existing data sources, gathering and maintaining the data needed, and completing and reviewing the collection of information. Send comments regarding this burden estimate or any other aspect of this collection of information, including suggestions for reducing this burden, to Washington Headquarters Services, Directorate for information Operations and Reports, 1215 Jefferson Davis Highway, Suite 1204, Arlington, VA 22202-4302, and to the Office of Management and Budget, Paperwork Reduction Project (0704-0188), Washington, DC 20503.

1. AGENCY USE ONLY (Leave blank)	2. REPORT DATE November 1993	3. REPORT TYPE AND DATES COVERED Technical Memorandum

4. TITLE AND SUBTITLE

Some VTOL Head-Up Display Drive-Law Problems and Solutions

5. FUNDING NUMBERS

533-02-37

6. AUTHOR(S)

Vernon K. Merrick

7 PERFORMING ORGANIZATION NAME(S) AND ADDRESS(ES)

Ames Research Center
Moffett Field, CA 94035-1000

8. PERFORMING ORGANIZATION REPORT NUMBER

A-93090

9. SPONSORING/MONITORING AGENCY NAME(S) AND ADDRESS(ES)

National Aeronautics and Space Administration
Washington, DC 20546-0001

10. SPONSORING/MONITORING AGENCY REPORT NUMBER

NASA TM-104027

11. SUPPLEMENTARY NOTES

Point of Contact: Vernon K. Merrick, Ames Research Center, MS 211-2, Moffett Field, CA 94035-1000
(415) 604-6194

12a. DISTRIBUTION/AVAILABILITY STATEMENT

Unclassified-Unlimited
Subject Category – 01

12b. DISTRIBUTION CODE

13. ABSTRACT (Maximum 200 words)

A piloted simulation test was conducted on the Ames Research Center's vertical motion simulator (VMS) in support of the Phase IIA flight test of NASA's V/STOL systems research aircraft (VSRA). During the simulation several problems were found with the head-up display (HUD) symbol drive laws and the flightpath synthesis. These problems and the solutions devised to solve them are described in this report. Most of the resulting HUD drive-law changes were implemented during the simulation and their effectiveness was verified. Subsequently both the HUD symbol drive-law and flightpath-synthesis changes were implemented in the VSRA and tested successfully in the Phase IIA flight tests.

14. SUBJECT TERMS

VTOL, Head-up display, Handling qualities

15. NUMBER OF PAGES

46

16. PRICE CODE

A03

17. SECURITY CLASSIFICATION OF REPORT Unclassified	18. SECURITY CLASSIFICATION OF THIS PAGE Unclassified	19. SECURITY CLASSIFICATION OF ABSTRACT	20. LIMITATION OF ABSTRACT